IMPROVEMENT OF THE FATIGUE STRENGTH PROPERTIES OF EN-AW 6082 ALUMINUM ALLOY BY MEANS OF DEEP ROLLING

EN-AW 6082 ALÜMİNYUM ALAŞIMININ YORULMA DAYANIMI ÖZELLİKLERİNİN DERİN OVALAMA VASITASI İLE İYİLEŞTİRİLMESİ

BERKAY YÜKSEL

Asst. Prof. MEHMET OKAN GÖRTAN
Supervisor

Submitted to
Graduate School of Science and Engineering of Hacettepe University
as a Fulfillment to the Requirements
for the Award of the Degree of Master of Science
in Mechanical Engineering

2022

ABSTRACT

IMPROVEMENT OF THE FATIGUE STRENGTH PROPERTIES OF EN-AW-6082 ALUMINUM ALLOY BY MEANS OF DEEP ROLLING

Berkay YÜKSEL

Master of Science, Department of Mechanical Engineering
Supervisor: Asst. Prof. Mehmet Okan GÖRTAN
May 2022, 47 Pages

In this study, fatigue properties of EN-AW 6082 aluminum alloy were altered using T6 heat treatment and deep rolling application. At first, artificial aging schedules were investigated and most optimal schedule for subsequent deep rolling was determined as 480min-180°C artificial aging preceded by 90min-550°C solution heat treatment and water quench. After artificial aging, axisymmetric specimens were subjected to deep rolling. This treatment allows one to induce compressive residual stresses in surface region of components. Effects of tensile loads during loading cycles can be reduced because of these compressive residual stresses. Deep rolling forces of 125 N, 250 N and 500 N were used with feed rates of 0.1, 0.2 and 0.3 mm/pass. Deep rolling was employed in two different directions. These directions were tangential rolling and longitudinal rolling. Conventional direction for deep rolling is tangential rolling in which rolling direction is tangent to turning direction and feed direction is in the direction of longitudinal axis of component. However, compressive residual stresses due to deep rolling are expected to be different in different directions as shown in literature. Therefore, a direction change in rolling is expected to change fatigue strength enhancement after deep rolling considerably. Surface states; namely: Roughness, hardness and residual stresses were measured for Un-treated, tangentially rolled and longitudinally rolled specimens. In addition, stress-controlled fatigue tests were conducted

to determine the effects of DR on fatigue behavior. It was shown that DR resulted in much lower roughness values than Un-treated for both rolling directions. However, increase of deep rolling feed rate affected roughness improvement adversely. Hardness values were shown to increase around surface after deep rolling for both rolling directions. This was especially true for 250 N and 500 N deep rolling forces. Up to 10% increase in hardness was obtained after deep rolling. Compressive residual stresses were shown to develop around the surface. Higher deep rolling forces resulted in higher maximum compressive stresses (more negative stresses) and depths at which maximum compressive stresses occur were shifted toward deeper into specimen. Different residual stress profiles for rolling and feed directions were observed. Higher compressive stress values near surface were detected in rolling direction after deep rolling. Fatigue tests showed that both tangential and longitudinal rolling increased fatigue strengths substantially compared to untreated specimens. However, fatigue strength increases were found to be higher for longitudinally rolled specimens than tangentially rolled ones. Fatigue strength increase of 26% could be achieved using longitudinal rolling procedure. In longitudinally rolled specimens, fatigue loading direction and rolling direction is the same. These results can be attributed to higher observed compressive residual stresses near the surface in rolling direction compared to feed direction. As a conclusion, it can be said that longitudinal rolling is an attractive option to improve fatigue properties of components in industrial applications.

Keywords: Deep Rolling, Mechanical Surface Treatment, Fatigue Life, Surface State

ÖZET

EN-AW 6082 ALÜMİNYUM ALAŞIMININ YORULMA DAYANIMI ÖZELLİKLERİNİN DERİN OVALAMA VASITASI İLE İYİLEŞTİRİLMESİ

Berkay YÜKSEL

Yüksek Lisans, Makine Mühendisliği Bölümü
Tez Danışmanı: Dr. Öğr. Üyesi Mehmet Okan GÖRTAN
Mayıs 2022, 47 Sayfa

Bu çalışmada, EN-AW 6082 alüminyum alaşımından üretilmiş parçaların yorulma dayanımları T6 temperi ve derin ovalama kullanılarak değiştirilmiştir. İlk olarak, farklı yapay yaşlandırma takvimleri kullanılarak malzemenin mekanik özelliklerinin yapay yaşlandırma parametrelerine bağımlılığı incelenmiştir. Bu incelemeler sonucunda optimum olarak 90 dk-550°C süper-doygun solüsyon oluşturma ve su verme işlemi sonrasında yapılan 480 dk-180°C yapay yaşlandırma seçilmiştir. Yapay yaşlandırma sonrası, eksenel simetrik parçalar derin ovalama işlemine tabi tutulmuşlardır. Bu işlem vasıtası ile yüzeyde baskı artık gerilmeler oluşması hedeflenmektedir. Oluşan baskı artık gerilmeler parka üzerindeki çekme yönündeki kuvvetleri azaltıcı etki yaptığından dolayı yorulma dayanımında olumlu etki ederler. Derin ovalama kuvveti olarak 125 N, 250 N ve 500 N; ilerleme hızı olarak da 0,1 mm/paso, 0,2 mm/paso ve 0,3 mm/paso uygulanmıştır. Derin ovalama işlemi, teğetsel ovalama ve boylamasına ovalama olmak üzere iki farklı yönde uygulanmıştır. Derin ovalama eksenel simetrik parçalar üzerinde geleneksel olarak teğetsel yönde yapılmakta ve ilerleme yönü de parçanın boyuna ekseni olarak seçilmektedir. Fakat, derin ovalama sonrası oluşan artık gerilmelerin her yönde aynı olmadığı literatürde gösterilmiştir. Bundan dolayı derin ovalama yönünün değiştirilmesinin yorulma dayanımı üzerinde belirgin bir etkisi

olacağı düşünülmektedir. Derin ovalama sonrası parçaların yüzey durumları, pürüzlülük, sertlik ve artık gerilme ölçümleri vasıtası ile belirlenmiştir. Yapılan tüm ölçümler; ovalanmamış, teğetsel ovalanmış ve boylamasına ovalanmış numuneler üzerinde yapılmıştır. Bu ölçümler sonrasında malzemelerin yorulma eğrileri ve dayanımları yapılan gerilme-kontrollü yorulma testleri vasıtası ile belirlenmiştir. Numuneler üzerinde yapılan pürüzlülük ölçümleri, her iki yönde yapılan derin ovalama sonrası elde edilen pürüzlülük değerlerinin ovalanmamış numunelere kıyasla oldukça düşük olduğu belirlenmiştir. Fakat, ilerleme hızının pürüzlülükteki iyileştirmeyi azaltıcı etkisi gözlenmiştir. Derin ovalama sonrasında yüzeye yakın bölgelerde sertlik artışı gözlenmiştir. Bu durum özellikle 250 N ve 500 N ile yapılan ovalamalarda belirgin bir almaktadır ve yüzeyde %10'a varan sertlik artışları elde edilebilmiştir. Derin ovalamaya bağlı baskı artık gerilmeleri her kuvvet için gözelenebilmiştir. Yüksek ovalama kuvvetleri baskı artık gerilmelerin ulaştığı maksimum değerleri (daha negative değerler) arttırmış ve daha derinde olmalarına sebep olmuştur. Ovalama ve ilerleme yönlerindeki baskı artık gerilmelerin farklı olduğu ve ovalama yönünde yüzey civarında daha yüksek baskı gerilmeler olduğu gözlenmiştir. Yapılan yorulma testleri sonucunda hem teğetsel hem de boylamasında ovalama yorulma dayanımlarını ovalanmamış numunelere kıyasla kayda değer miktarda iyileştirmiştir. Fakat, boylamasına ovalamanın yorulma dayanımında olan olumlu etkilerinin daha belirgin olduğu gözlenmiş ve %26'ya varan yorulma dayanımı artışları rapor edilmiştir. Boylamasına ovalamada, ovalama yönü yorulma testlerindeki yükleme yönü ile aynı yöndedir. Ovalama yönünde yüzey civarında elde edilen yüksek baskı artık gerilmeler dikkate alındığında; artık gerilme ölçümleri ile yorulma davranışları birbirini destekler niteliktedir. Elde edilen bulgular, boylamasına ovalamanın endüstriyel uygulamalarda yorulma dayanımını iyileştirmek için kullanılabileceğini göstermiştir.

Keywords: Derin Ovalama, Mekanik Yüzey İşlemleri, Yorulma Ömrü, Yüzey Durumu

ACKNOWLEDGEMENTS

I would like to thank to my valued supervisor Asst. Prof. Dr. Mehmet Okan Görtan for his patience, guidance and tireless assistance during the preparation of this thesis;

I also thank The Scientific and Technological Research Council of Turkey (TÜBİTAK) for financially supporting this study under the project number 217M962.

I would also like to thank my fiancée Sena Gizem Bodur for her supports during my studies.

Finally, I thank my precious family who always encouraged and supported me throughout my life and during preparation of this study with their endless love and patience. Without their encouragements, preparation of this thesis would not be possible.

Berkay Yüksel
May 2022, Ankara

CONTENTS

LIST OF FIGURES

LIST OF TABLES

1. INTRODUCTION

Regulations on greenhouse gases and emission standards are becoming tighter for automotive industry [1]. Therefore, automotive manufacturers should produce lightweight vehicles without compromising safety in order to reduce fuel consumption. For this reason; usage of lightweight materials and/or less material usage became prominent. Usage of aluminum alloys as an alternative to steels for manufacturing of dynamically loaded components has been increasing in automotive industry as stated in [2]. Heat-treatable EN-AW 6xxx series aluminum alloys are especially used for manufacturing of dynamically loaded parts such as wheel suspension arms.

Since the cause of mechanical failures in modern machinery is predominantly fatigue [3], it is important to improve fatigue properties of dynamically loaded components. Initiation of fatigue cracks usually occurs in surface region due to defects at surface [4]. Reducing surface roughness is known to be beneficial for fatigue strength as stated in the work of Kirkhope et al. [5], since reduced roughness decreases notch effect and impedes crack initiation. Introducing compressive residual stress layer at surface region also allows for improvement in fatigue strength [6]. Because, fatigue failure requires tensile loads and compressive residual stresses reduces the applied tensile loads on components so that crack initiation and propagation can be hindered. Mechanical surface treatments which enhances these surface properties of components can be used to increase fatigue strength. Main mechanical surface treatment methods are; shot peening (SP), laser shock peening (LSP) and deep rolling (DR) as designated in reference book on the subject [7]. Since deformation on component is not homogenous after these treatments, compressive residual stresses can be obtained near-surface region if appropriate process parameters are used.

Shot peening process is applied using high velocity shots made of steel or ceramic to peen the material surface for a predetermined time and intensity [8]. In the work of Maio et al. [9], fatigue strength of 2024 aluminum alloy specimens were increased up to 28% after shot peening treatment. However, shot peening generally affects surface topography negatively, since peening occurs randomly and as a result some deep valley may form after treatment [10]. Laser shock peening process relies on short laser pulses of some nanoseconds to peen material surface [11]. This process provides an opportunity for peening of surface in a more

controlled manner compared to shot peening. Deeper compressive residual stresses were observed for laser shock peening than shot peening [12]. In addition to that, surface roughness increase after laser shock peening was shown to be less than it was after shot peening [13]. Deep rolling is applied on components using ball or roller shaped apparatus. Application of load may be ensured employing either hydraulic or mechanical (by use of springs) principles [7]. Compared to shot peening and laser shock peening, deep rolling results in deeper compressive residual stresses up to 1 mm depth compared to 0.2 mm for shot peening and 0.8 mm for laser shock peening as reported in [14]. Substantial hardness increase in surface region was observed by Richards et al. [15] up to 1.3 mm depth after deep rolling. Apart from these effects, deep rolling reduces surface roughness; which in turn reduces notch effect at surface and hinder crack initiation [16]. Reduction of roughness is a distinctive advantage of deep rolling over shot peening and laser shock peening.

Because of the effects explained above, mechanical surface treatments are viable options to improve fatigue strength properties. Shot peening is the oldest and most traditional method and allows for complex shapes to be processed. However, reduction in surface quality after shot peening possess a significant problem in terms of fatigue strength properties. Laser shock peening requires a significant capital investment in the order of million-dollar-plus as indicated by a manufacturer [17]. On the other hand, deep rolling tools are cheap; and rolling operation can be performed on already existing conventional or CNC lathes. The fact that roughness is reduced and deep compressive residual stresses form after deep rolling; combined with economical advantage, allows for significant improvement of fatigue strength for industry. In this work, EN-AW 6082 aluminum alloy was used in T6 condition. This alloy is commonly used in automotive industry for manufacturing of dynamically loaded components such as wheel suspension arms. Firstly, a preliminary study was performed to investigate effects of T6 heat treatment parameters on mechanical properties, since there was no standard procedure on the subject. After that, deep rolling was applied on manufactured specimens. Surface state alterations and fatigue strength enhancements after deep rolling were compared to study the effect of deep rolling parameters on fatigue strength properties of EN-AW 6082 aluminum alloy.

2. STATE OF THE ART

2.1. Heat Treatment

EN-AW 6xxx series aluminum alloys; sometimes referred as Al-Mg-Si alloys, are heat-treatable and commonly used in T6 condition [18]. T6 heat treatment consists of solution heat treatment above 500°C, rapid quenching and subsequently artificially aging (AA) at temperatures above 130°C for a pre-determined time to obtain precipitation hardening response; thus increasing strength [19-21]. Precipitates responsible for hardening has a complex forming sequence which was well explained by [22-23]. In essence, a supersaturated solid solution (SSSS) is obtained after solution heat treating and quenching. Obtained solid solution consists of quenched-in vacancies and dislocations that allows for nucleation and growth of meta-stable needle shaped β″ precipitates during artificial aging. This precipitate is the main hardening phase for precipitation hardening of 6xxx alloys. An increased delay after quenching reduce effectiveness of subsequent artificial aging; therefore, time between quenching and artificial aging should be minimized to obtain highest performance from heat treatment [19]. Because, clusters containing Mg and Si forms in SSSS at room temperature and these clusters occupies quenched in vacancies, which are normally needed for β″ nucleation. Therefore, precipitate nucleation becomes less likely or even impossible. Apart from this, excessive artificial aging time was shown to cause over-aging, which reduces strength as aging progresses. This effect is more pronounced and significantly faster in high temperature applications than lower temperature ones [21]. Reason for this is transformation of β″ to β′ precipitate. Because of these reasons, it can be said that peak-age condition for AA is a strong function of both temperature and time.

2.2. Fatigue Behavior

Fatigue failure of metals has been noticed since 1830s. Metal components that were loaded well below the strength required to fracture in a fluctuating manner were observed to fail [24]. Since fatigue failures usually occurs without external warning, it possesses a severe risk for economic losses, injuries and deaths. Therefore, investigation of fatigue strength behavior is critical. First systematic investigation on fatigue was conducted by August Wöhler [25] in 1870 who at the time worked as railway engineer. His study on fatigue of railway axles is an example of stress-controlled fatigue testing in which load on specimen is held constant throughout fluctuating loadings until fracture. Other method for fatigue testing

is strain-controlled test as shown in [26] in which strain on specimen held constant throughout test until fracture. Generally, high cycle fatigue (HCF) behavior where life until fracture is above 10^4 cycles are determined using stress-controlled tests whereas low cycle fatigue (LCF) behavior for fracture below 10^4 cycles is determined strain-controlled tests [24]. Fatigue tests can be done without mean stress/strain (fully reversed), with mean stress/strain or in an irregular manner as shown in Figure 1.

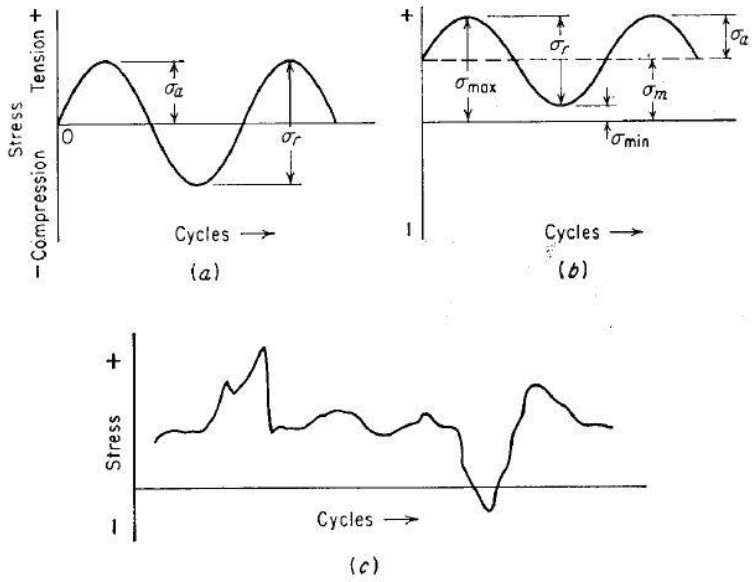

Figure 1 Typical Stress Controlled Fatigue Cycles (a) Fully Reversed (b) With Mean Stress (c) Irregular Stress Cycle [24]

Fatigue of metals can be divided into 4 segments: Crack nucleation, micro-crack propagation, macro-crack propagation and final fracture as shown in Figure 2 [27]. Initial nucleation of fatigue crack happens on high shear stress planes where plastic strain accumulates and results in persistent slip bands (PSB) as fluctuation continues [28]. In micro-crack propagation or Stage-I crack growth; high shear stress planes of persistent slip bands deepen and form a micro-crack [29]. After a critical crack length, crack growth direction changes to be perpendicular to applied maximum tensile load, which is called macro-crack propagation or Stage II crack growth. After macro-crack propagation, a sufficiently long crack causes material to fail catastrophically under last loading cycle since not enough material is left to resist loading. Generally, most of the life is spent on Stage-II crack growth in LCF whereas most of the life is spent on Stage-I growth for HCF [24].

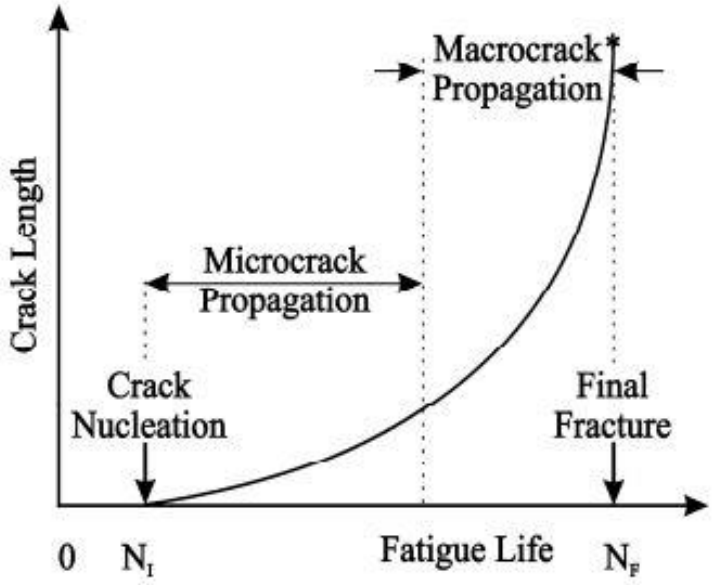

Figure 2 Fatigue Life Stages [27].

2.3. Surface Treatment Methods

Mechanical surface treatments can be applied on components to improve surface-region properties, since fatigue properties are prone to surface-region state of a material. Three mechanical surface treatment methods, namely; shot peening, laser shock peening and deep rolling were discussed in this section.

2.3.1. Shot Peening

Shot peening process involves accelerated shot of high hardness made of steel, ceramic or glass to peen material surface [8]. During collision between shot and workpiece, a portion of kinetic energy of the shot results in a local plastic deformation at workpiece surface and purely elastic deformation under a critical length. When the shot leaves the surface, elastically deformed section cannot recover completely because of the plastically deformed layer at surface and generates residual compressive stress state at surface [30]. By peening the whole surface thoroughly, a uniform compressive residual stress state can be achieved. Maio et al. [9] reported compressive stresses reaching to 0.5 mm in cast iron specimens after shot peening. As a result, they achieved 31% fatigue strength improvement. However, shot peening inherently increases surface roughness, which is unfavorable for fatigue strength. In addition, selection of inappropriate process parameters may result in crack-like defects as shown by Bagherifard et al. [10].

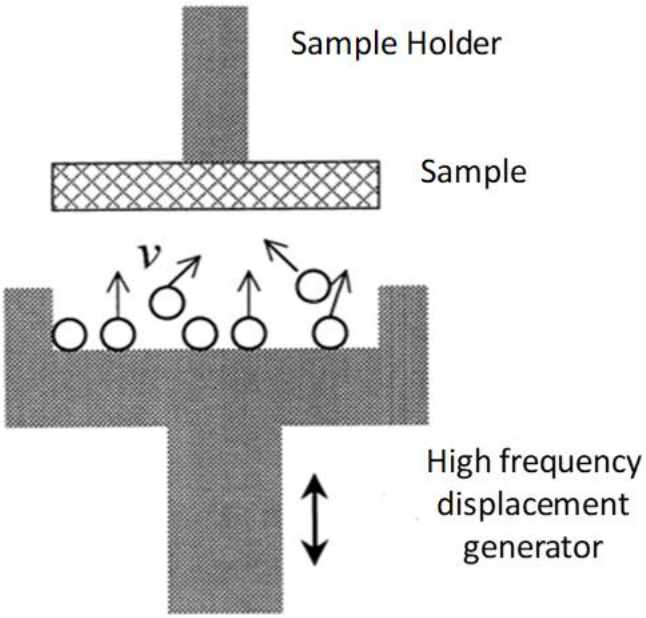

Figure 3 Schematic Representation of Shot Peening [31]

2.3.2. Laser Shock Peening

Laser shock peening employs laser pulses instead of shots. In order to apply LSP, surface to be peened is painted and a water layer is used as a transparent overlay. When the laser pulse interacts with the paint, paint transforms into plasma by expanding and creating a high-pressure shock. This shock stage lasts some nanoseconds and causes workpiece surface to deform plastically, which results in compressive residual stress state at surface [11]. Schematic representation of LSP can be seen in Figure 4.

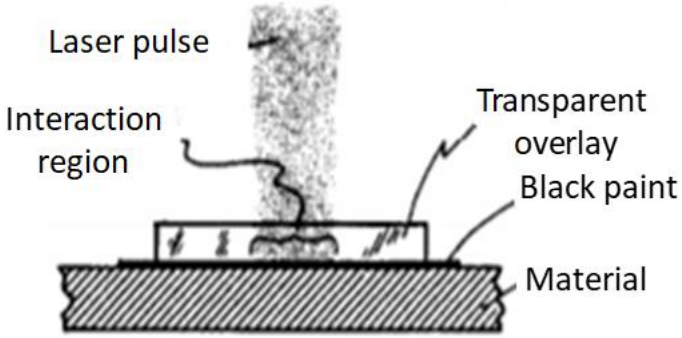

Figure 4 Schematic Representation of Laser Shock Peening [11]

Laser shock peening has been generally applied in aviation industry [32-33]. Dane et al. [32] applied LSP on Inconel 718 and obtained compressive residual stresses reaching up to 1 mm compared to 0.5 mm for SP. This alloy commonly used for manufacturing of turbine blades

of jet engines. Nalla et al. [33] applied LSP on Ti-6Al-4V and obtained considerable fatigue strength improvement. However, this improvement was less than it was for deep rolling.

2.3.3. Deep Rolling

Deep rolling is applied on workpiece surface using hydraulically or mechanically supported ball or roller with a predetermined force, feed rate and rolling speed [34]. An example of the process can be seen in Figure 5. Deep rolling force (p), feed (f_r) and rolling speed (v_r) were shown on the figure. Deep rolling is expected to result in three main enhancements: hardness increase at surface, decrease in roughness and compressive residual stress layer near surface. Alterations at surface are usually determined using either experimental of numerical methods. Sufficiently accurate analytical methods to predict residual stresses could not be derived; due to complex 3-dimensional nature of the process [7].

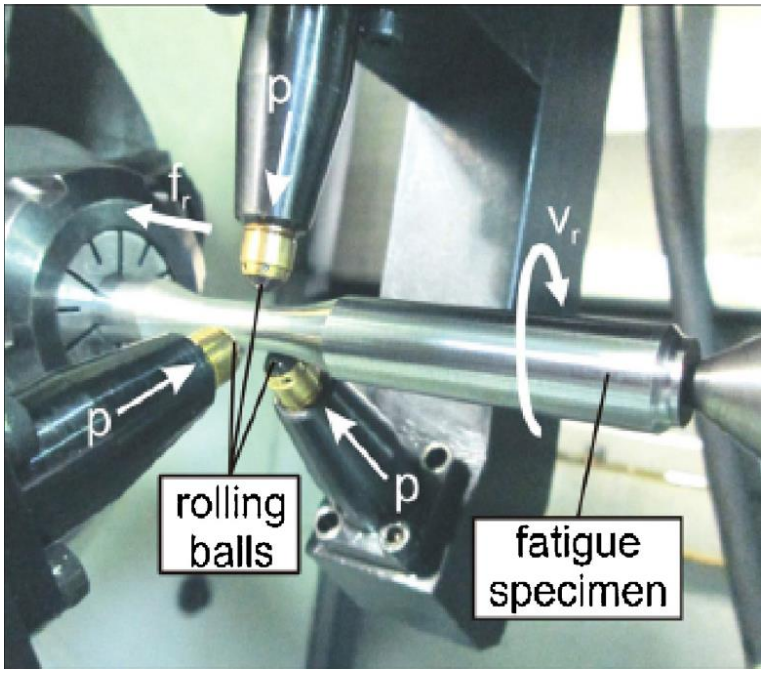

Figure 5 Deep Rolling Using Hydraulically Supported Balls [34]

Hardness increase due to work-hardening in surface-region is known to be beneficial for fatigue strength [6]. Increased hardness means higher resistance to plastic deformation. Therefore, higher hardness is expected to hinder crack initiation by reducing plastic strain accumulation. Abrao et al. [36] reported 37% hardness increase at surface after deep rolling for a carbon steel. Similarly, Abdulstaar et al. [37] reported 21% hardness increase at surface

for 6082 aluminum alloy. In the same study, it was shown that hardness increase at surface was higher for DR than it was for SP.

Deep rolling reduces surface roughness by deforming the ridges at surface and flattening them. Beghini et al. [38] reported reduction of average roughness (R_a) from 0.65 μm to 0.28 μm. They also showed that roughness obtained after deep rolling was a strong function of roughness value before deep rolling. As a result of reduction in roughness, fatigue strength increases because of reduced notch effect [6]. If rolling force exceeds a certain level, surface roughness improvement can be reduced. Therefore, care should be practiced to determine rolling force [7].

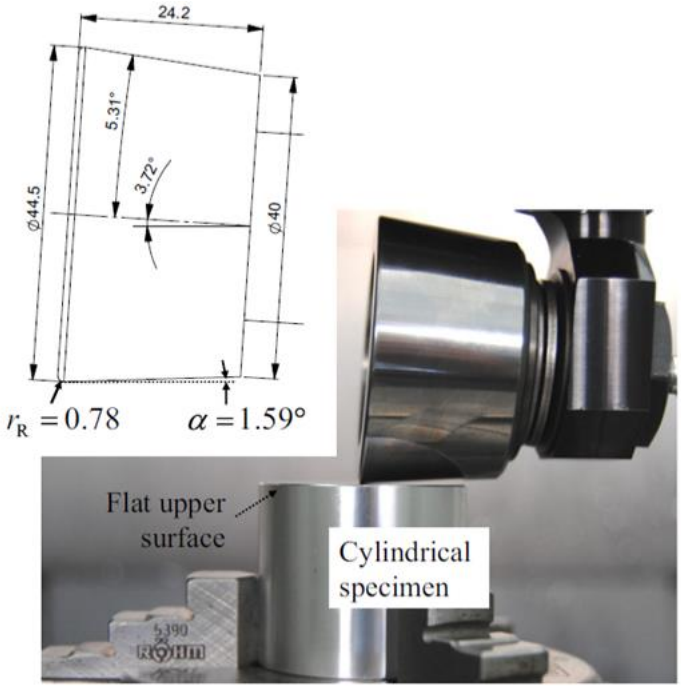

Figure 6 Deep Rolling Using Mechanically Supported Roller [38]

Compressive residual stresses formed after deep rolling is the most important effect after deep rolling. Sticchi et al. [39] reported 5 times deeper compressive residual stresses were formed after DR compared to SP. Compressive residual stresses which can reach up to 1 mm depth were reported by several research groups [37-39].

Due to reasons listed above, fatigue strength improvements in the range of 20% and 300% were reported in literature [37, 40-41]. DR can be applied in a controlled and homogenous

manner; therefore, can be used in manufacturing of components of high-added value such as turbine blades of jet engines [42].

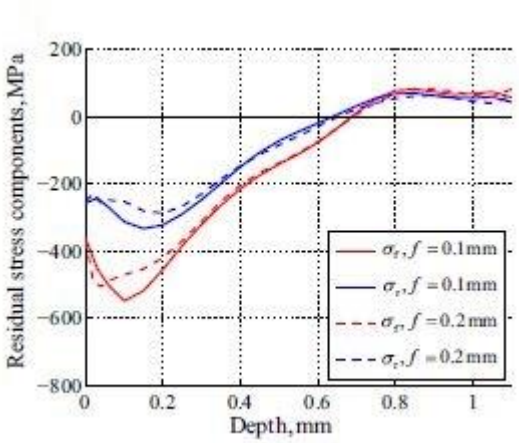

Figure 7 Residual Stress Measurements in Different Directions for Different Feeds [38]

Recent studies showed that residual stresses formed after deep rolling were not same in every direction after DR. DR on 7075 aluminum alloy resulted in higher compressive residual stresses at surface in feed direction than rolling direction in the work of Beghini et al. [38]. Their deep rolling geometry and residual stress measurement results were shown in Figure 6 and 7, respectively. In Figure 7, σ_r and σ_f are residual stresses in rolling and feed direction, respectively. Residual stresses in feed direction were almost twice as much as residual stresses in rolling direction. Similarly, Wong et al. [35] showed different residual stresses in different directions for Ti-6Al-4V alloy after DR. Coules et al. [43] investigated 3-dimensional residual stresses after DR and showed that residual stresses after DR were in fact dependent on direction. All of these works were conducted on flat-surface specimens. However, components in industry are generally either axisymmetric or involving some radii. DR on axisymmetric components was conventionally applied in such manner that rolling direction is tangential to turning direction and feed direction is in the direction of longitudinal axis of workpiece [7]. However, residual stress profiles are expected to be different in these two directions after deep rolling. Therefore, changing DR direction is expected to influence fatigue behavior considerably for axisymmetric parts. Longitudinal rolling, in which the rolling direction is in the longitudinal axis direction of component was not reported in literature before.

Fig. 8 shows fatigue lives of EN-AW 7075 aluminum alloy for different conditions. For 130 MPa stress amplitude, deep rolling (regarded as roll-peening in the figure) yielded best results whether rolling force was low or high. Approximately 1,500,000 cycles were reached for high-force roll-peening compared to 200,000 cycles for fretting fatigue and 650,000 cycles for shot-peened samples. As stress amplitudes increased, shot peened samples became better in terms of fatigue life. For example, at 280 MPa stress amplitude shot-peened samples exhibited approximately 200,000 cycles compared to 100,000 for roll-peened samples. This is the result of more stable work-hardened layer after shot peening than deep rolling as was suggested in [7]. In order to improve stability of deep-rolled surface, deep rolling can be done with multiple passes to saturate the surface state. Nevertheless, deep rolling was still found to be attractive for low-stress high-cycle applications.

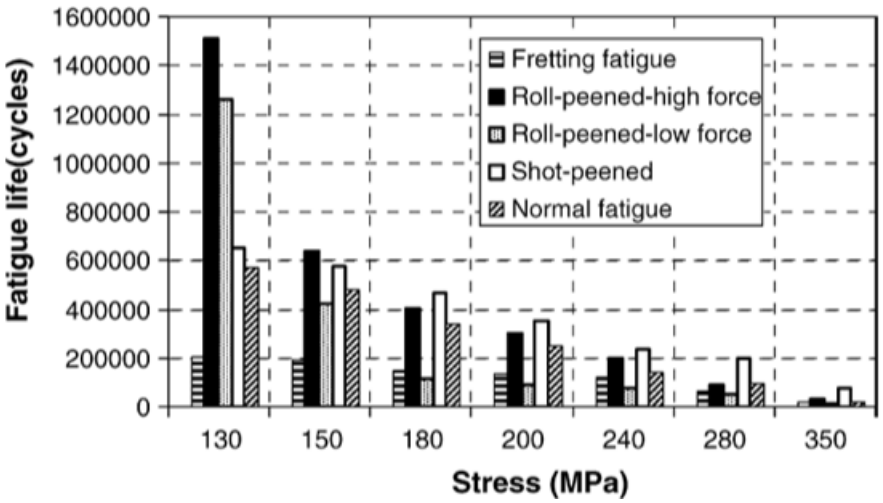

Figure 8 Different Applications and Fatigue Life Data for 7075 Aluminum Alloy [47]

3. NOVEL APPROACH

Literature survey showed that for asymmetric parts, deep rolling in tangential directions as shown in Figure 9(a) is conventional application of DR. Longitudinal rolling direction was not reported for deep rolling in literature before. However, different residual stresses form after deep rolling when roller type tool is used. Therefore, effect of deep rolling direction on fatigue strength of axisymmetric parts was investigated in this study using un-treated (UT), tangentially rolled (TR) and longitudinally rolled (LR) specimens.

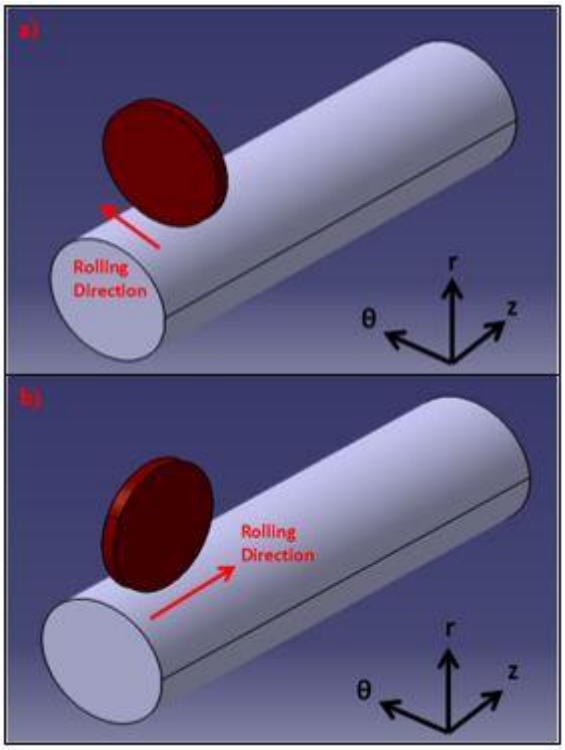

Figure 9 Deep Rolling Directions (a) Tangential Rolling (b) Longitudinal Rolling

4. METHODS AND PRELIMINARY INVESTIGATIONS

This section is dedicated to explain experimental and analytical methods used in this work. In addition to that, preliminary investigation regarding the T6 heat treatment of EN-AW 6082 Aluminum Alloy was also presented.

EN-AW 6082 aluminum alloy bars of 15 mm diameter and 1 m length were supplied. Chemical analysis results supplied by manufacturer was presented in Table 1. In order to manufacture specimens, 1 m bars were cut into 120 mm long pieces and all test specimens were produced using these pieces.

Table 1 Chemical Composition of EN-AW 6082 Aluminum Alloy [wt.%]

Si	Fe	Cu	Mn	Mg	Cr	Zn	Ti	Al
0.93	0.295	0.015	0.53	1.00	0.0055	0.083	0.012	97.2

4.1. Mechanical Behavior Investigations

In order to determine mechanical behavior, tensile tests were carried out in accordance with DIN50125:2009-07 standard. Tests were done using type-A specimens with 8 mm gage diameter and 40 mm gage length (DIN 50125 – A 8 x 40). Tensile test specimen geometry can be seen in Figure 10(a). Tests were conducted on a servo-mechanical UTEST testing machine at room temperature. Strain rate was $1x10^{-3}$ [mm/mm]. For every tensile test condition, 3 specimens were tested and results were averaged. For hardness measurements, specimens were ground using successive grit-papers of 240-400-1000-2500 μm followed by polishing with 6 μm and 1 μm diamond solutions. Hardness tests were conducted using Future-Tech FM-700e Vickers Hardness tester. ISO 6507-1 standard was used as a reference for hardness tests. When hardness of bulk of the material interior was to be measured, 500 g load was used. However, when hardness measurements of surface regions were needed, 10 g load was used to capture more spatial resolution with hardness tests. In all of the cases 15 s dwell time was employed.

Fatigue properties were investigated using stress-controlled fully reversed (R=-1) cycles in high cycle fatigue region. ASTM E466-07 standard was used as reference for conducting fatigue tests. Fatigue test specimen geometry can be seen in Figure 10(b). Tests were done using servo-hydraulic BESMAK axial fatigue test machine at 5 Hz. For stress-controlled

fatigue investigation; different stress amplitudes are applied on specimens in a fluctuating manner for fully reversed stresses until specimen fracture. After each specimen failure, fatigue life of corresponding specimen is recorded. Recorded fatigue life is dependent variable. After all of the test has finished, recorded fatigue lives are plotted together with stress-amplitudes. Wöhler curves (S-N diagrams) in the form of equation (1) are to be derived. In equation (1), S_a is stress amplitude selected, N_f is fatigue life until failure, $S_f^{'}$ is fatigue strength coefficient and b is the fatigue strength exponent. Constants $S_f^{'}$ and b are derived using least squares regression method and Wöhler curves are formed. These curves show how much life can be expected for a given stress amplitude for components.

$$S_a = S_f^{'}(N_f)^b \tag{1}$$

Since fatigue behavior exhibits significant scatter, other statistical methods were employed to derive lower bounds for Wöhler curves. These methods were lower 3-sigma and Owen one-sided tolerance limits. Procedure for calculation of these lower bounds explained in [44]. Both of these methods relies on calculation of standard error of experimental data set around Wöhler curve. Afterwards, this standard error is multiplied with some constant number and subtracted from Wöhler curve. For lower 3-sigma, aforementioned constant is taken as 3. However, for Owen one-sided tolerance limit, this constant is a function of sample size, desired reliability and confidence interval. Determined constants can be found on some reference studies [45]. In the current study, 90% reliability and 90% confidence interval was used for Owen one-sided tolerance limits.

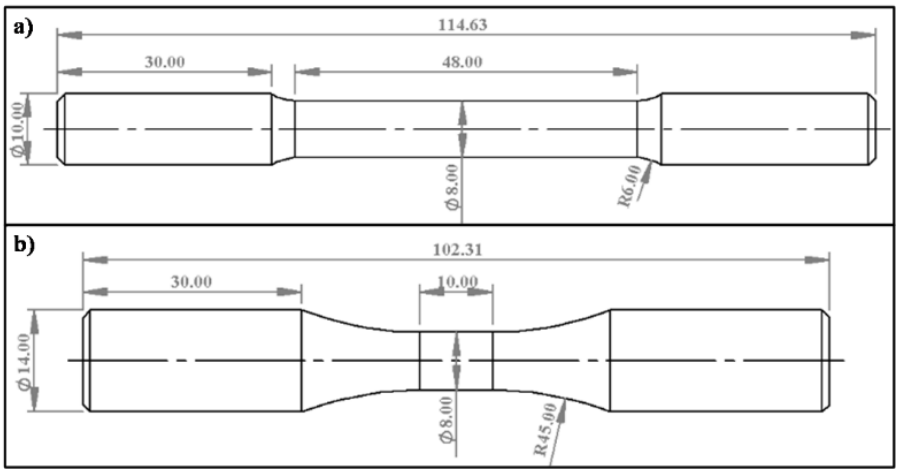

Figure 10 Test Specimens (a) Tensile test specimen (b) Fatigue test specimen

4.2. Preliminary Heat Treatment Investigations

Heat treatment procedure to obtain T6 condition in EN-AW 6082 aluminum alloy was investigated and presented in this section. T6 heat treatment starts with solution heat treatment (SHT) generally above 500°C followed by rapid quenching to obtain supersaturated solid solution (SSSS). After quenching, artificial aging (AA) is applied to obtain meta-stable β″ precipitates. This precipitate is the main hardening precipitate and therefore desirable. General precipitation sequence was suggested as [22]:

SSSS → solute clusters → small spherical precipitates→ needle-shaped β″ → β′ → β

Effects of SHT temperature, AA temperature and time were investigated to reveal the dependency of mechanical properties on T6 temper parameters.

4.2.1. Effect of Solution Heat Treatment Temperature

In order to investigate the effect of solution heat treatment temperature on precipitation behavior, three SHT temperatures; 500°C, 525°C and 550°C were applied on specimens for 90 minutes and specimens were quenched subsequently. Afterwards samples with 4 mm diameter and approximately 24 mg mass were prepared using standard metallographic procedures for every SHT condition. DSC analyses were performed on prepared samples using Hitachi DSC 7020 machine between room temperature and 350°C with heating rate of 10°C/min. Apart from DSC analyses, tensile tests for artificially aged specimens for every SHT condition were performed. AA was applied 480min-180°C for this investigation.

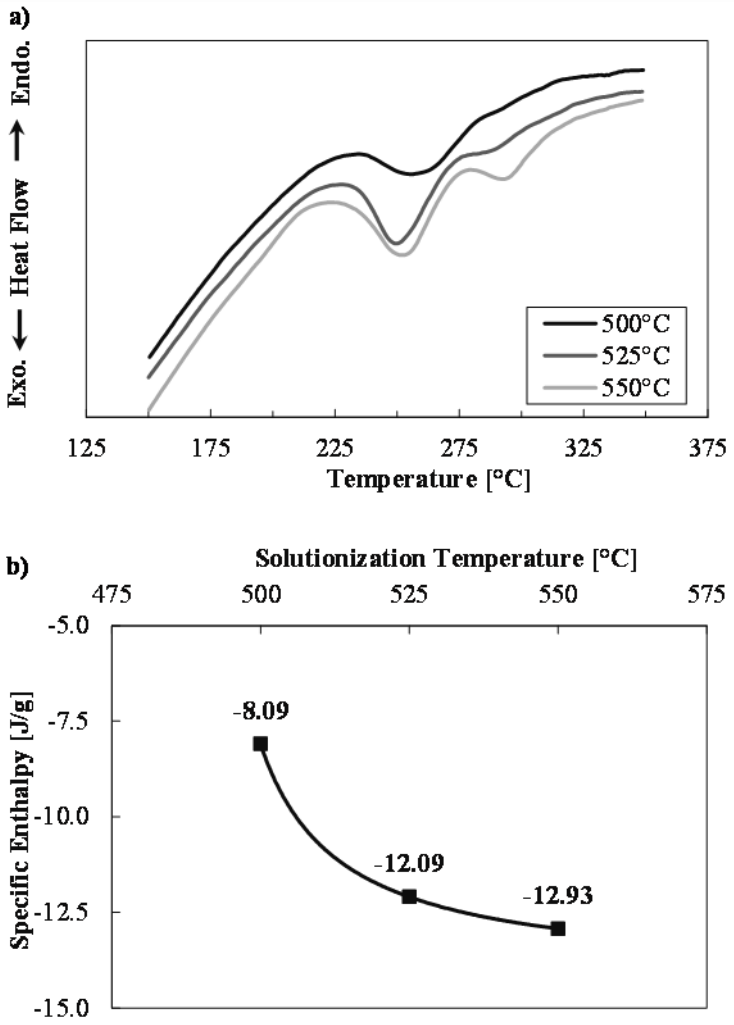

Figure 11 DSC Results (a) DSC Curves of Specimens that were Solution Heat Treated at Different Temperatures (b) Specific Enthalpy Changes Calculated for Peak around 250°C

Figure 11(a) shows that as SHT temperature increased, starting point of exothermic peak around 250°C shifted towards lower temperatures and peak intensity has increased. This peak is associated with formation of β″ precipitate [46]. This shows that higher SHT temperatures results in more favorable SSSS condition for β″ precipitate to nucleate. In addition, specific enthalpy changes corresponding to exothermic peak around 250°C has increased in magnitude as can be seen in Figure 11(b); meaning more precipitate could nucleate. Tensile test results after 480min-180°C AA were shown in Table 2 for different SHT conditions. Yield strength (σ_y) and ultimate tensile strength (σ_{UTS}) values seen in Table 2 confirms the DSC results. As SHT temperature increased, obtained yield strength values increased from 287.8 MPa to 298 MPa for 500°C and 550°C, respectively. Similar trend was

also observed for ultimate tensile strengths. In addition, standard deviations shown in Table 2 also decreased for higher temperature SHT, hence increasing reliability. Therefore, 550°C temperature was found to be an appropriate temperature to carry out SHT and used as SHT temperature throughout the current study.

Table 2 Strength Values for Different SHT Temperatures after 480min-180°C AA

	500°C	525°C	550°C
σ_y [MPa]	287.8±22.7	284±8.23	298±5.41
σ_{UTS} [MPa]	305.4±22.5	304.1±5.0	318.9±5.2

4.2.2. Effect of Artificial Aging Schedule on Mechanical Behavior

Effects of artificial aging temperature and time on mechanical properties of EN-AW 6082 aluminum alloy was investigated using temperatures between 180°C-230°C and aging times of 60-120-240-480 minutes. In order to investigate temperature dependence, 10°C increments were used in AA schedules. Schematic representation of investigated AA schedules can be seen in Figure 12.

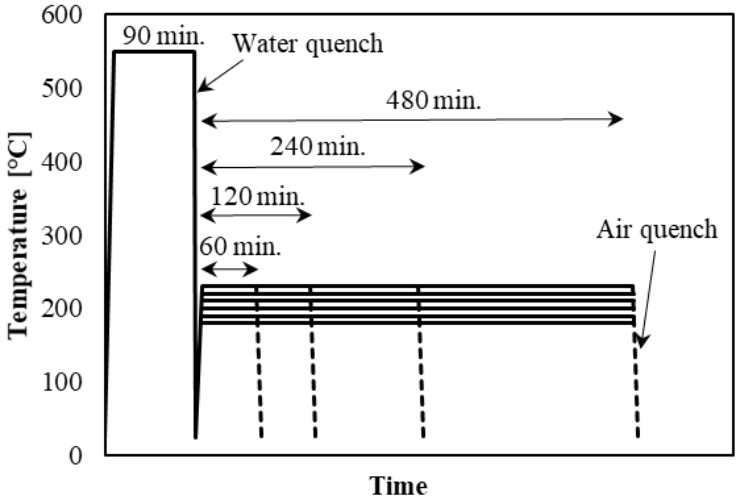

Figure 12 Schematic Representation of AA Schedule

Figure 13 shows strength values obtained from tensile tests after AA treatments. It can be seen in Figure that peak-age time reduced as AA temperatures increased. For example, peak-age yield strength of 315 MPa was found for 240min-200°C AA compared to 306 MPa yield strength found for 60min-220°C AA. It is important to note that real peak-age conditions can be in between data points. Nevertheless, effect of temperature on age-hardening response can be realized with ease. In all of tested temperatures, peak-age yield strength values were

in a small range between 298 MPa and 315 MPa. Therefore, it can be said that peak-age yield strength value is not affected significantly by AA temperature; rather time to get peak-age response is affected by it. For temperatures T ≥ 200°C, over-aging observed where strength values decrease after peak-age point as AA continues. For example, yield strength was reduced from 310 MPa to 289 MPa from 240min to 480 min AA at 210°C. Tensile strength results show parallelism to yield strength behavior and peak-age conditions followed by over-aging were observed on tensile strengths as well.

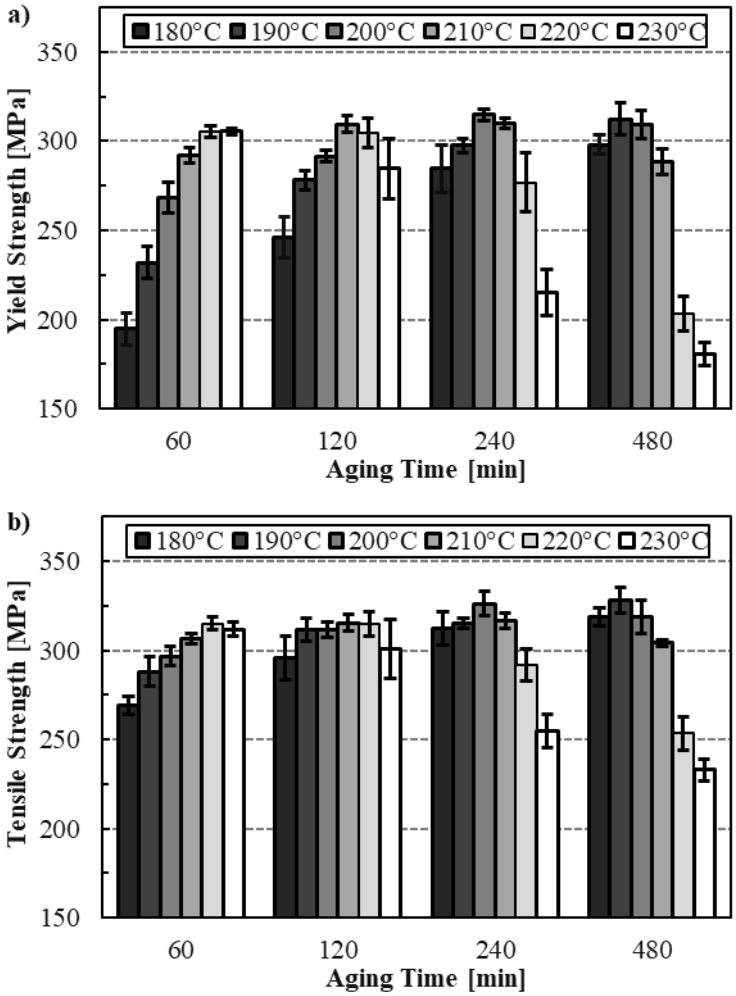

Figure 13 Strength Values for AA treatments (a) Yield Strength (b) Tensile Strength

Hardness values obtained for each AA condition were presented with corresponding tensile strength values in Figure 14. As can be seen, a linear relationship with a sufficient efficiency can be established. Correlation coefficient of $R^2 \approx 0.96$ was found. This value indicates scatter of data was minimal and proposed linear relationship was accurate. Slope of the line was found to be approximately 2.3.

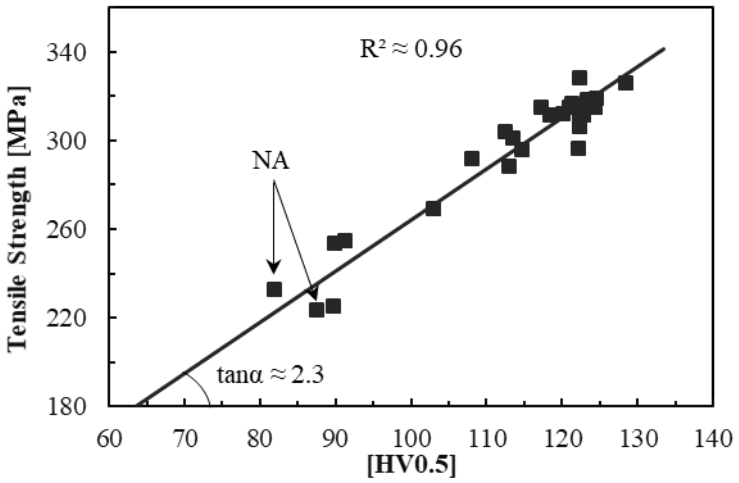

Figure 14 Relationship between Hardness and Tensile Strength; Natural Aging (NA) Specimens were also presented

Figure 15 shows elongation behavior for different AA treatments. Elongations reduced as artificial-aging progressed up to peak-age condition as expected. Uniform elongation of 5% and total elongation of 15% were satisfied at peak-age condition for every AA procedure. However, elongation increase during over-aging was not at the level that was expected. Over-aged specimens showed both lower elongation and strength values than under-age and/or peak-age specimens. For example, 240min-230°C AA yielded lower yield strength than 60min-190°C AA as seen in Figure 14. However total elongation for 240min-230°C AA was 20% whereas it was 26% for 60min-190°C. These results are compatible with results of [21] who reported lower fracture toughness values for over-aged samples than under-aged ones for same strength level. Therefore, it can be said that over-aging has a negative effect on ductility of 6082 aluminum alloy.

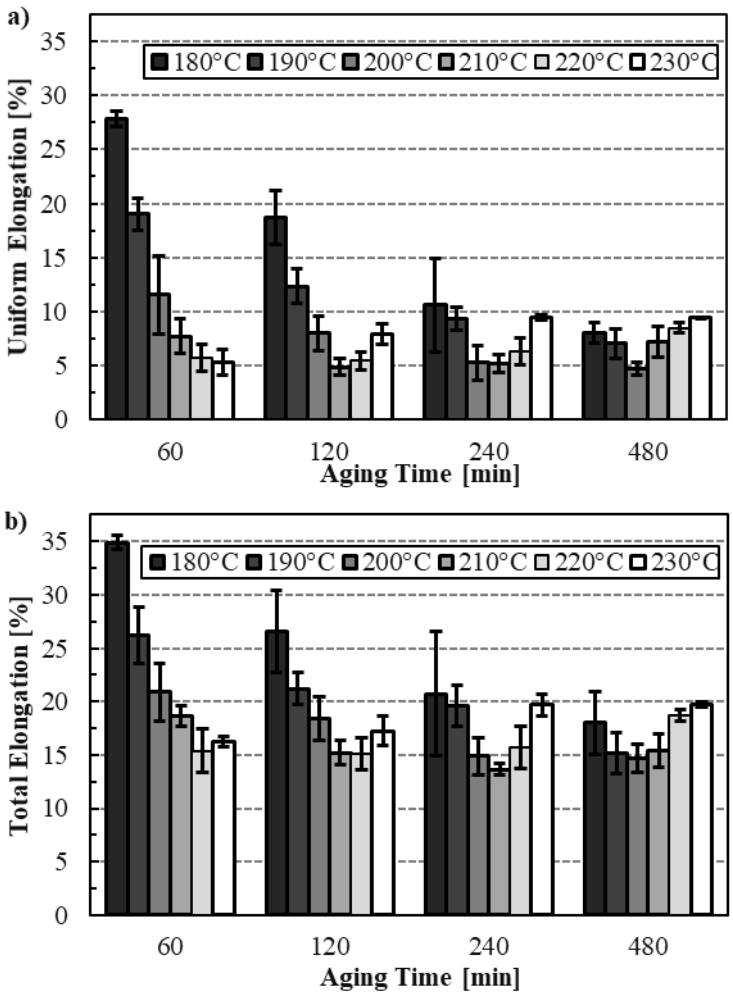

Figure 15 Elongations for AA treatments (a) Uniform Elongation (b) Total Elongation

Fatigue properties were investigated for two AA conditions. 480min-180°C AA is a common practice in industry and 240min-200°C AA had highest yield strength of 315 MPa in the current study. As can be seen in figure 16, application of 240min-200°C AA instead of 480min-180°C had no adverse effect on high cycle fatigue behavior. In fact, there was a slight improvement in fatigue strength by applying 240min-200°C. This is not surprising since tensile strength of 240min-200°C AA was higher than 480min-180°C AA. Fatigue strength at 10^6 cycles were 162 MPa and 159 MPa for 240min-200°C and 480min-180°C, respectively.

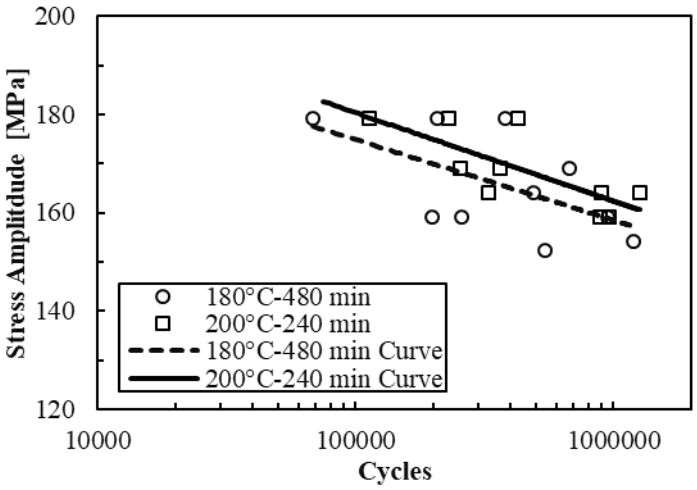

Figure 16 Fatigue Properties of Selected AA Treatments

4.2.3. Effect of Artificial Aging Schedule on Precipitate Formation

Precipitates formed during aging were investigated using transmission electron microscopy. Specimens of 8 mm x 8 mm squares were prepared with a thickness of 300 µm. Afterwards, 3 mm diameter disks were punched from these specimens and thinned using twin-jet electropolishing with nitric acid solution. Examinations of TEM were made using JEOL JEM-2100 electron microscope.

Figure 17 and 18 show TEM micrographs of 480min-180°C AA and 240min-200°C, respectively. Both cases exhibited both spherical precipitates and needle-shaped β″ precipitates. Average sizes of precipitates and corresponding standard deviations were presented in Table 3. Both precipitate types were larger for 240min-200°C than 480min-180°C. Measured β″ length for 480min-180°C AA was consistent with the study of Cuniberti et al. [19] who measured 17.6 nm length for β″ for 240min-180°C. In the same work, 30 minutes of AA at 180°C resulted in 14 nm length for β″ precipitates. This shows that there was only 3.6 nm (25%) increase in length from 30 minutes to 240 minutes AA. Therefore, for the current study, 17.2 nm length of β″ precipitates for 480min-180°C are not expected to increase considerably with further AA. On the other hand, 240min-180°C AA resulted in 21.3 nm length for β″. This suggests that AA temperature has a significant effect on final β″ precipitate length at peak-age condition.

Table 3 Size Measurements of Precipitates

	Diameter (Spherical) or Length (β″) [nm]	
	180°C-480 min	200°C-240 min
Spherical	11.0 ± 0.8	14.4 ± 2.7
β″	17.2 ± 2.1	21.3 ± 2.4

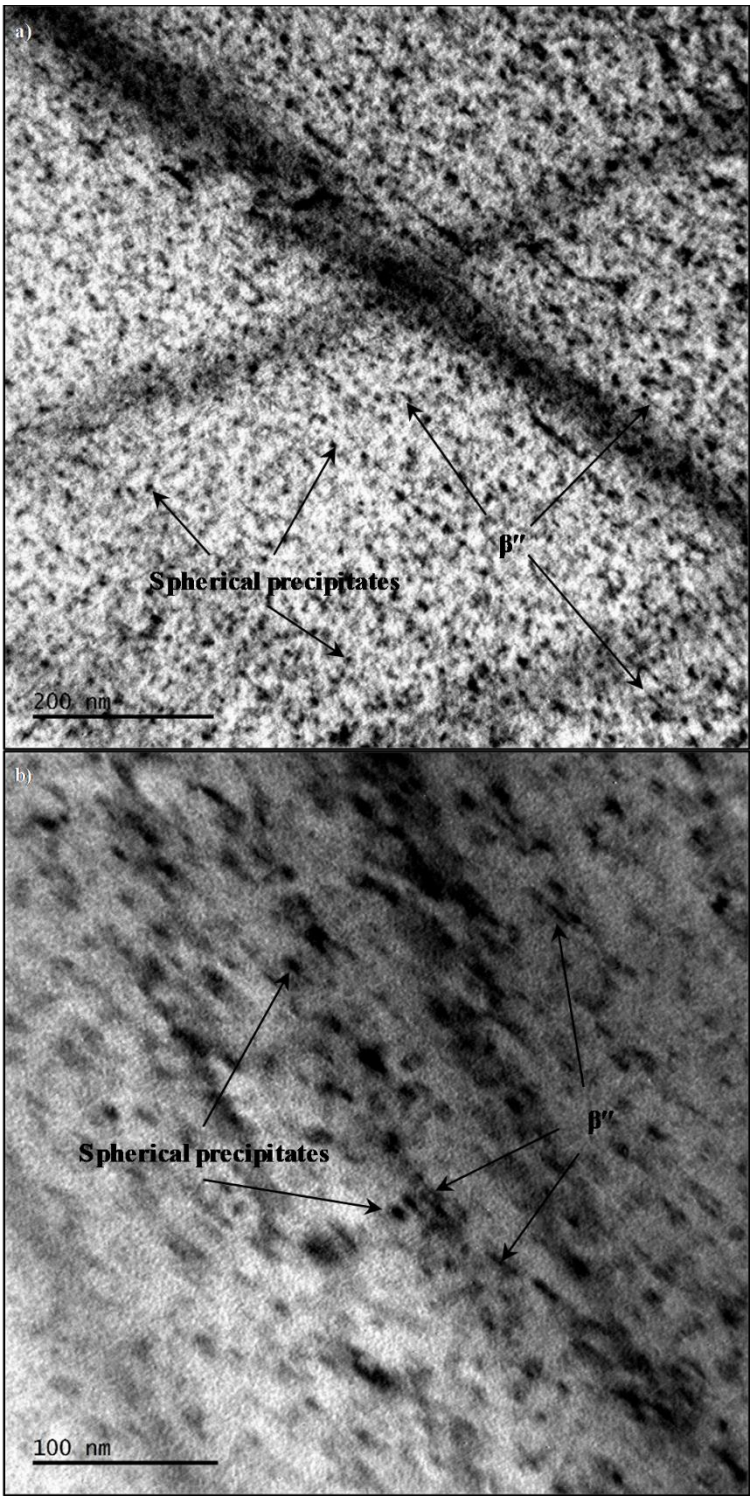

Figure 17 TEM Images of 480min-180°C AA specimen

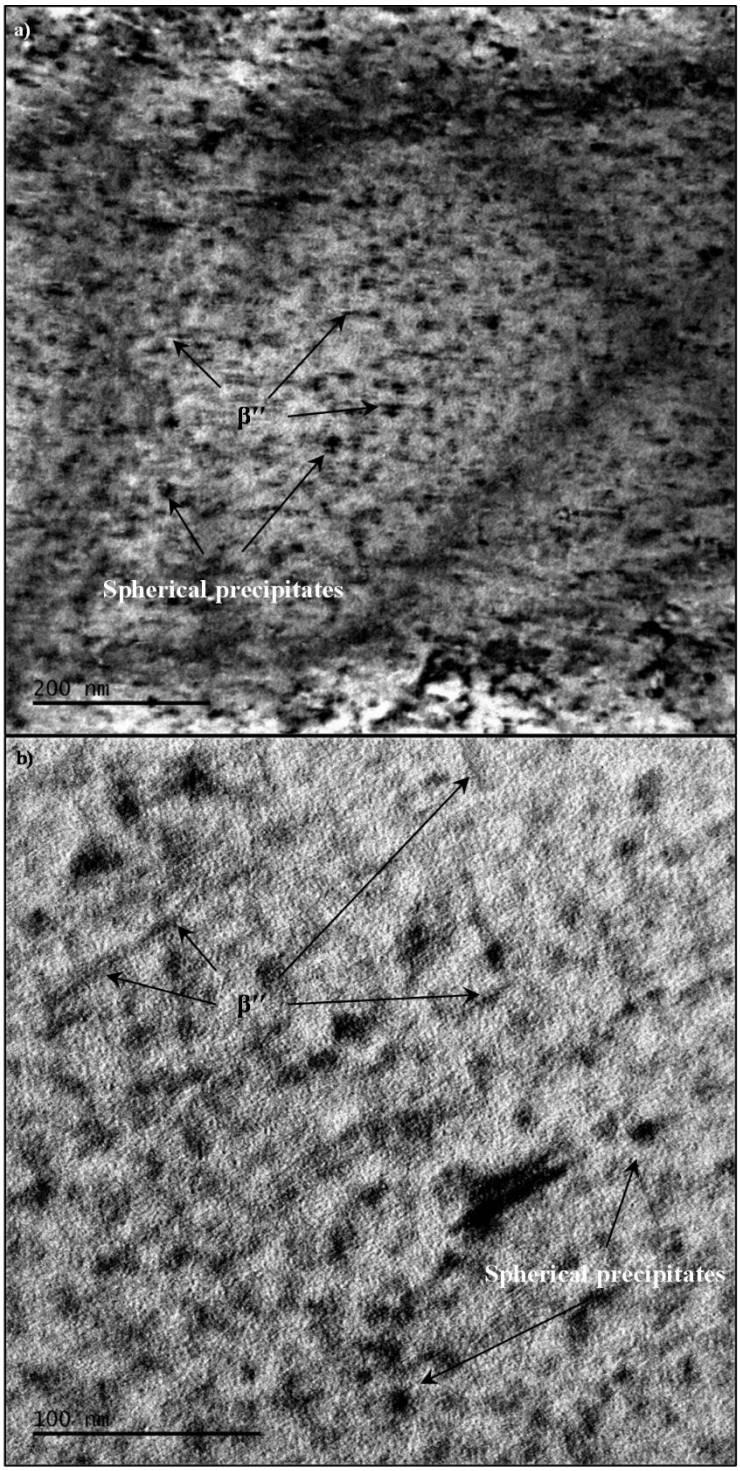

Figure 18 TEM Images of 240min-200°C AA specimen

4.2.4. Selection of T6 Treatment Procedure

Figures 13 and 14 show that 480min-180°C AA resulted in ultimate tensile strength higher than 300 MPa (319 MPa) and exhibited a sufficient uniform elongation of 8%. Uniform elongation is critical for deep rolling since surface of the specimen is stretched in deep rolling

and some degree of ductility is needed. Therefore, 480min-180°C AA was used in subsequent investigations.

4.3. Manufacturing of Deep Rolling Specimens

Several types of specimens were manufactured to investigate the effects of deep rolling on specimens. Deep rolling was performed using Yamato SKUV20-2.5R-A80 model deep rolling tool. It has 85 mm roller disk diameter and 2.5 mm tip radius. Load application of DR tool is provided by spring within the tool. This spring is loaded using hex key for a predetermined amount. Hex key screw on deep rolling tool was shown in Figure 19. For investigations, three forces were applied for deep rolling; 125 N, 250 N and 500 N. Rolling speed was selected as 10 mm/s for all applications. Feed rates of 0.1 mm/pass, 0.2 mm/pass and 0.3 mm/pass were employed.

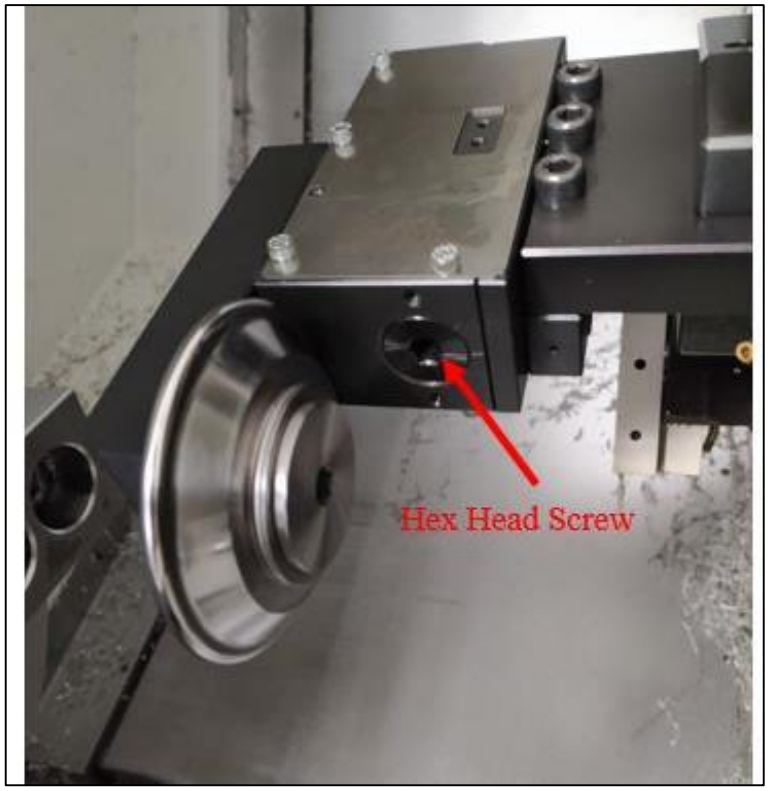

Figure 19 Deep Rolling Tool and Hex Head Screw to Load Spring within

In order to manufacture a flat surfaced specimen using a milling machine out of 15 mm diameter bar, a fixture was designed to hold the bar as can be seen in Figure 20. Fixture was subjected to grinding to obtain the net final shape accurately. Using this fixture, flat specimens were manufactured in a standardized manner.

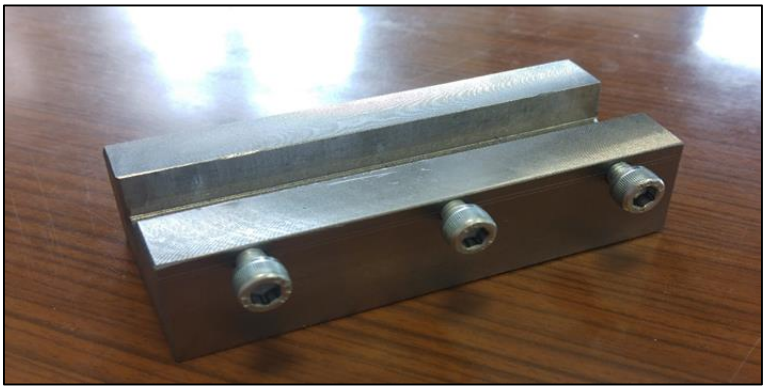

Figure 20 Fixture Designed to Manufacture Flat Surface Specimen

Deep rolling of Flat surface was shown in Figure 20. Flat specimens with a width of 11.6 mm were manufactured and subjected to deep rolling for roughness and residual stress measurements. Rolling and feed directions were shown in Figure 20.

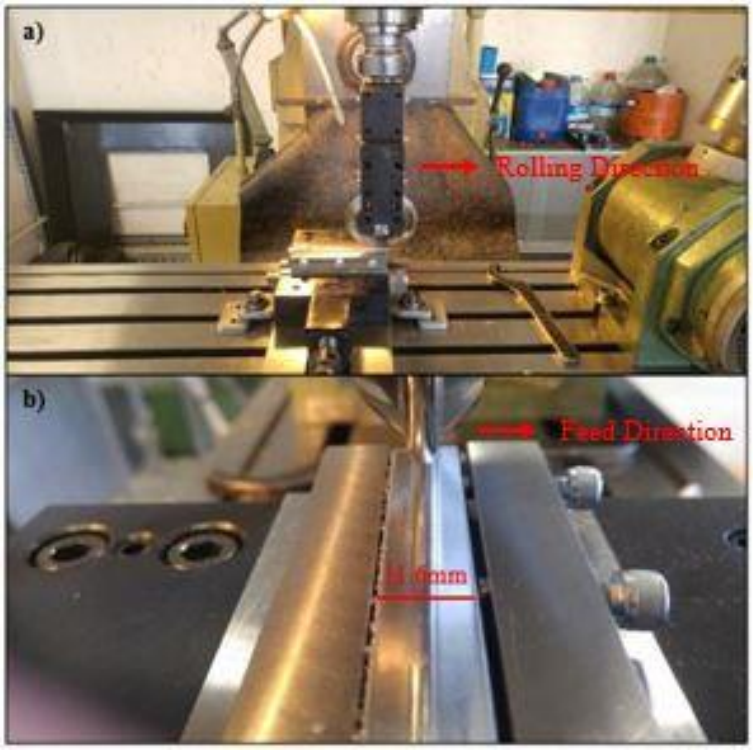

Figure 21 Deep Rolling of Flat Specimen (a) Side-view (b) Front-view

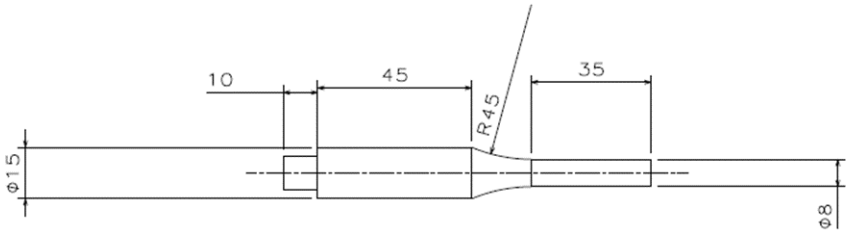

Figure 22 Cylindrical Roughness Measurement Specimen; Dimensions in mm.

Geometry of cylindrical specimens for roughness measurements were shown in Figure 22. These specimens were subjected to deep rolling in tangential and longitudinal direction as shown in Figure 23(a) and 23(b), respectively. Likewise, application of deep rolling on fatigue specimen was shown in Figure 24. Geometry of fatigue specimens was already shown in Figure 10(b) under the section 3.1. 45 mm radius corner were used in order to be able to conduct longitudinal rolling in gage section completely, since deep rolling tool has 42.5 mm roller radius.

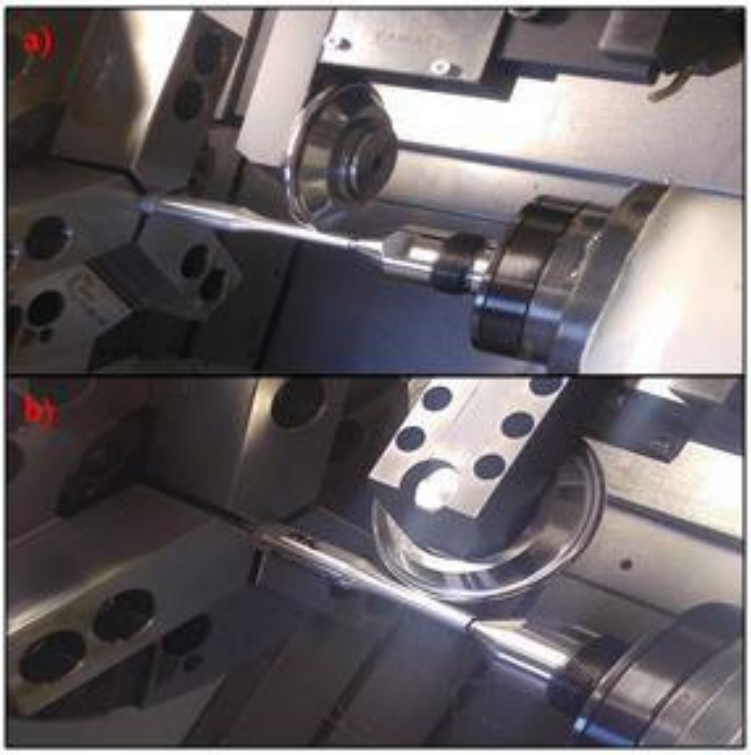

Figure 23 Deep Rolling of Cylindrical Roughness Specimen (a) Tangential (b) Longitudinal

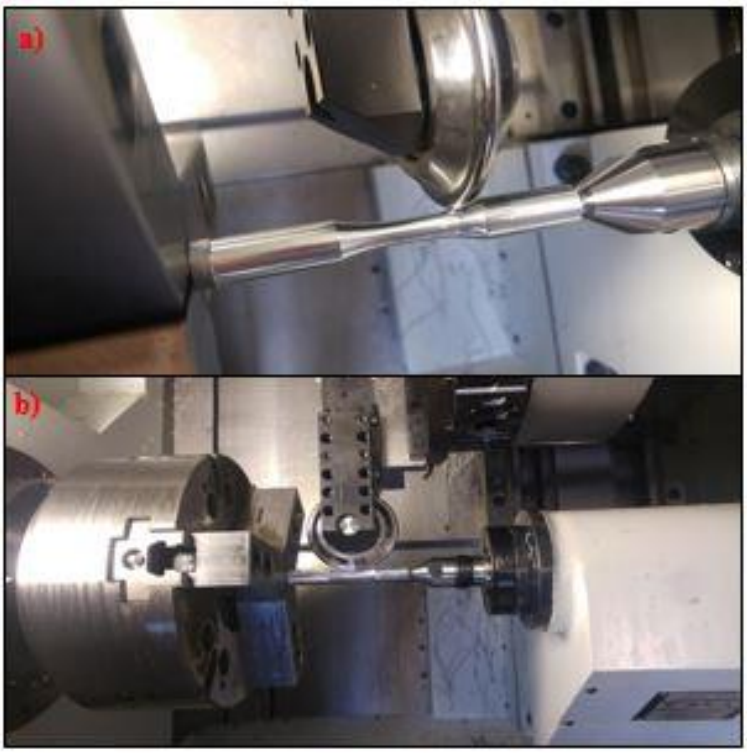

Figure 24 Deep Rolling of Fatigue Specimens (a) Tangential (b) Longitudinal

4.4. Roughness Measurements

Roughness measurements of specimens were conducted in accordance with ISO 4287-1997 standard. Both Ra (average roughness) and Rz (ten-point maximum roughness) Measurements were measured. Measurements were done using Mitutoyo SJ-210 skidded stylus roughness device. All the measurements were done in the direction of longitudinal axis of specimens. Measurements in tangential direction for cylindrical specimens were not possible, because the measuring device was skidded. Roughness measurements of curved surfaces can be done using skidless stylus instruments. At least 10 measurements were done for each case and roughness values were averaged. Roughness measurement configuration was shown in Figure 25.

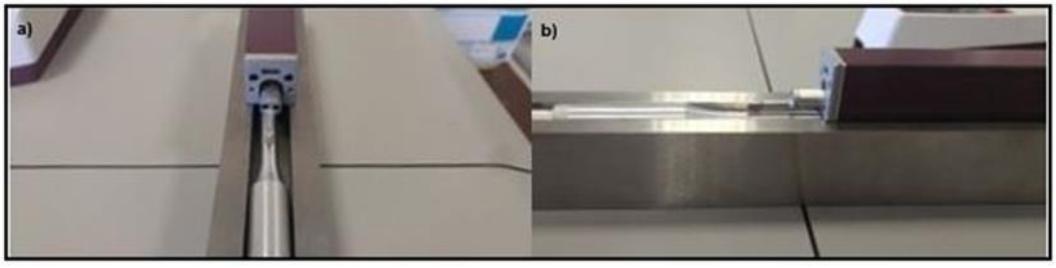

Figure 25 Roughness Measurement Configuration (a) Front-view (b) Side-view

4.5. Residual Stress Measurements

Residual measurements were done using hole drilling method (HDM) according to ASTM E837-08 standard. Measurements were done on flat specimens since curved specimens yield erroneous results with this method. In this method, a hole is drilled with successive steps onto specimen and strains were recorded using strain gages for each step. Schematic representation of a strain gage type was shown in Figure 26.

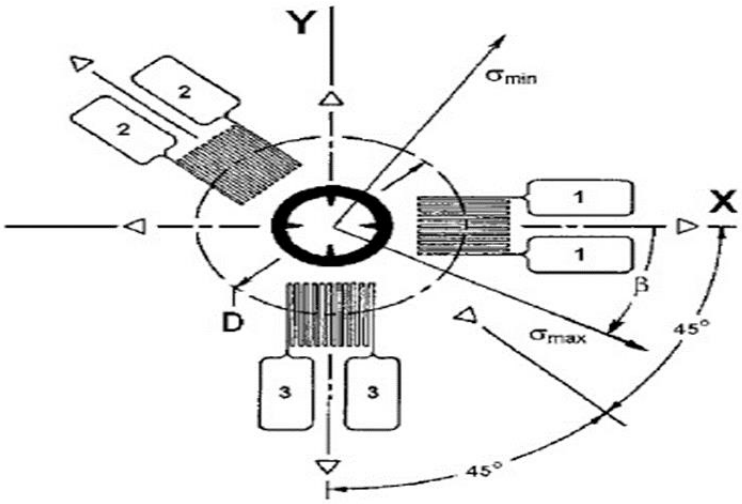

Figure 26 Type-A 031-RE Strain Gage for HDM [ASTM E837-08]

In this study, x-direction of strain gage shown in Figure 26 was aligned with specimens' longitudinal directions as shown in Figure 27. Diameter of the hole to be drilled was 1 mm. Maximum measurable depth is 0.5 mm for this case. In practice however, after 0.4 mm measurement results became unreasonable. Therefore, measurements were done up to 0.4 mm depth using 6 measurement steps. Drill bit turning speed was 15000 rev/min and feed rate was 1 μm/s. In order to be able to drill the hole in correct position, two perpendicular cameras were employed and positioning was done using these cameras. Measurement system can be seen in Figure 28.

Figure 27 Strain Gage on Specimen

Using the strain recordings after each step, corresponding strain vectors can be obtained as below;

$$p_j = (\varepsilon_3 + \varepsilon_1)_j/2 \quad (2)$$

$$q_j = (\varepsilon_3 - \varepsilon_1)_j/2 \quad (3)$$

$$t_j = (\varepsilon_3 + \varepsilon_1 - 2\varepsilon_2)_j/2 \quad (4)$$

Using a_{jk} and b_{jk} constants supplied in ASTM E837-08, below equations can be solved in matrix form. Bold characters represent vector or matrix quantities;

$$\bar{\mathbf{a}}\,\mathbf{P} = \frac{E}{1+v}\,\mathbf{p} \quad (5)$$

$$\bar{\mathbf{b}}\,\mathbf{Q} = E\,\mathbf{q} \quad (6)$$

$$\bar{\mathbf{b}}\,\mathbf{T} = E\,\mathbf{t} \quad (7)$$

Cartesian stress components can be calculated using obtained vectors as follows;

$$(\sigma_x)_j = P_j - Q_j \quad (8)$$

$$(\sigma_y)_j = P_j + Q_j \quad (9)$$

$$(\tau_{xy})_j = T_j \quad (10)$$

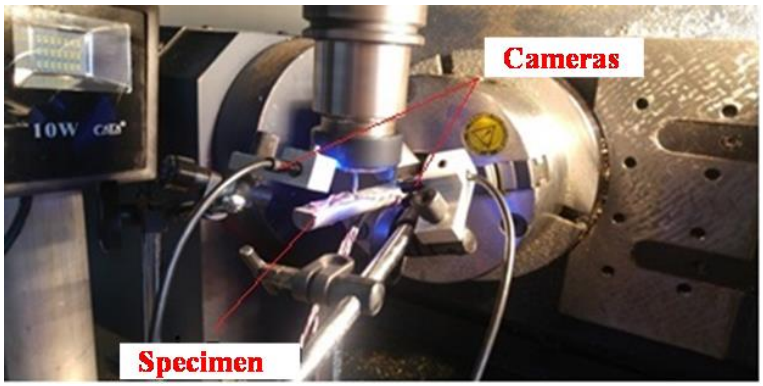

Figure 28 Residual Stress Measurement System

5. RESULTS

Experimental results of this work were presented under this section. Roughness, hardness, residual stress and fatigue property alterations were all discussed under separate sections.

5.1. Roughness Results

Roughness values of tangentially rolled (TR) 8 mm diameter cylindrical specimens were presented in Figure 29 for different DR forces and feeds. Results of untreated (UT) specimen were presented as well. For every DR parameter, both Ra and Rz values were decreased compared to UT specimen and there was no adverse effect. Feed rate had a significant effect on roughness values. In contrast, dependence of Ra and Rz on DR force was small for the same feed rate. For example, at 0.1 mm/pass feed rate, 125 N force resulted in 0.08 μm Ra compared to 0.1 μm for 500 N. Difference between them was negligible since UT specimen Ra was 0.72 μm and significant improvement was made after DR. A similar trend was observed for Rz as well.

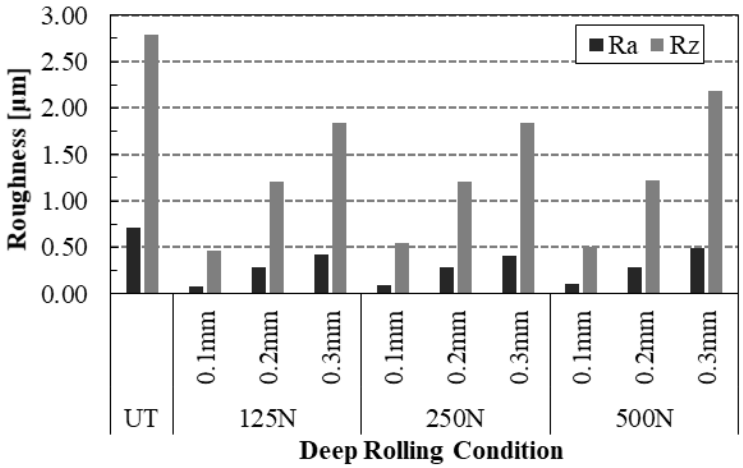

Figure 29 Roughness Values for TR Specimens

Figure 30 shows roughness values of longitudinally rolled (LR) specimen set. Similar to TR set, for all DR conditions, roughness values were improved compared to UT specimen. Feed rate had more influence over Ra and Rz values than force as it was in TR. However, force had more pronounced effect for LR than for TR. For example, at 0.1 mm/pass feed rate, Ra value for 125 N was approximately 3 times of the value for 500 N; 0.202 μm for 125 N compared to 0.064 μm for 500 N. Similar trend was observed for Rz.

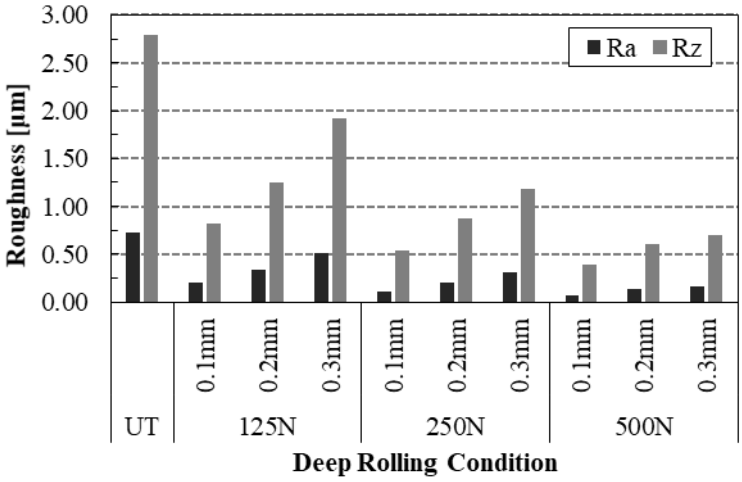

Figure 30 Roughness Values for LR Specimens

5.2. Hardness Results

Hardness measurements to investigate work-hardening at surface region were done for 8 mm diameter 0.1 mm/pass specimens. Figure 31 shows hardness measurements of specimens with DR forces 125 N, 250 N and 500 N were shown. Black lines represents bulk material hardness of 123.1 HV. According to Figure 31(a), hardness distribution of 125 N resulted a minor change in hardness, only limited to close proximity of surface. For 250 N and 500 N, hardness increases were more pronounced.

For 250 N DR, TR and LR did not result in any significant difference in hardness distributions and for both cases; hardness increase reached approximately 0.8 mm depth. Approximately 10% increase in hardness values were obtained close to surface for 250 N.

For 500 N DR, there was an observable hardness behavior difference between TR and LR. TR resulted in more pronounced hardness increase than LR. In TR, contact area is smaller than LR. Because of this, higher stresses develop in surface region and more plastic deformation occurs than LR; hence more work-hardening. Hardness increase reached approximately 1 mm depth.

These results showed that considerable work-hardening was obtained using DR whether it was TR or LR. Especially for 250 N and 500 N DR, work-hardened surface layer was achieved. This is beneficial for fatigue strength since hardness increase is expected to hinder fatigue crack initiation.

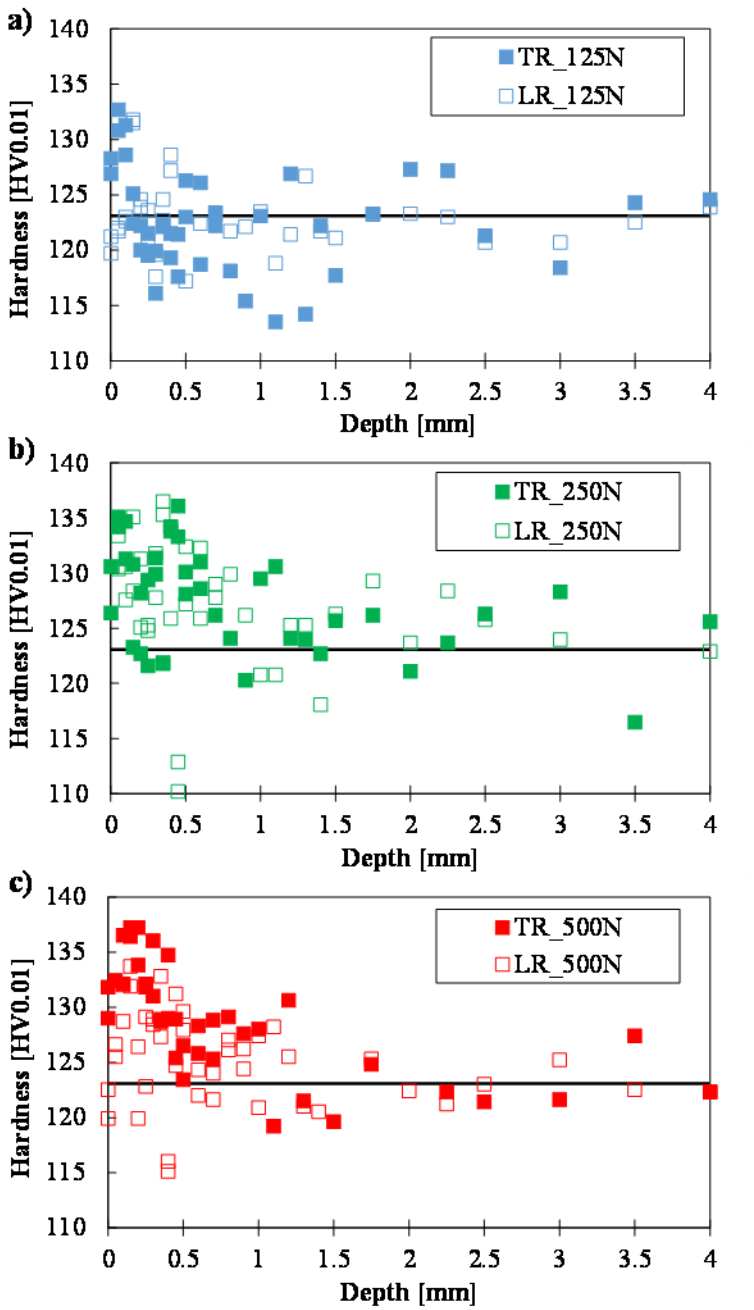

Figure 31 Hardness Measurements after DR with 0.1 mm/pass Feed (a) 125 N (b) 250 N (c) 500 N

5.3. Residual Stress Results

Residual stress profiles for flat surface DR specimens were shown in Figure 32. 0.1 mm/pass feed rate was used for all forces. For every DR force, compressive residual stresses were observed near-surface region. Residual stresses showed a decreasing trend toward a minimum value at first, and then increased afterwards. Minimum residual stress (maximum compressive) location got deeper as DR forces increased. For 500 N DR, residual stress trend

toward the surface shows that residual stress values were higher (more tensile) at surface. This affect fatigue strength negatively, since fatigue cracks generally initiates at surface. Residual stresses at depths more than 0.4 mm could not be measured. Compressive residual stresses near surface should be balanced by tensile stresses at interior. Because of this, higher tensile residual stresses are expected in deeper regions for higher DR forces, since compressive residual stresses near surface reduced as DR forces increased. This can result in crack initiation at maximum tensile residual stress locations and increased crack propagation speed at these locations for existing cracks.

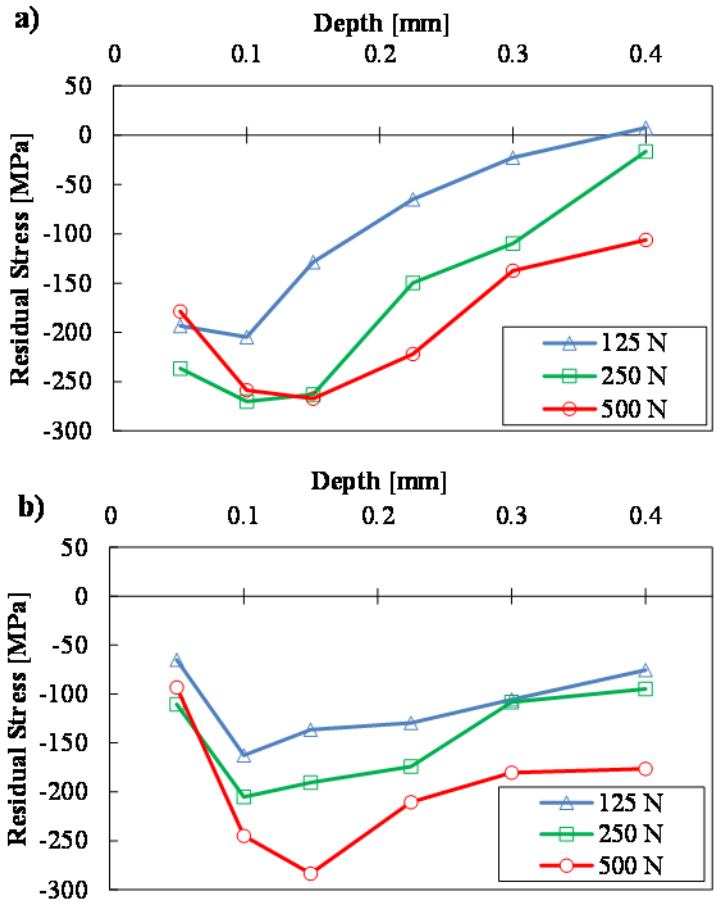

Figure 32 Residual Stress Profiles of Flat DR Specimens (a) Rolling Direction (b) Feed Direction

5.4. Fatigue Test Results

Fatigue tests were conducted using at least 10 specimens for each case. Figure 33 shows Wöhler curves obtained after DR using 0.1 mm/pass feed together with UT specimens. Experimental data points were not presented because of the clarity of the figure. Both TR and LR resulted in considerable fatigue strength increase compared to UT. This is the

combined result of reduced roughness, increased hardness and compressive residual stresses at surface for deep rolled specimens compared to un-treated ones.

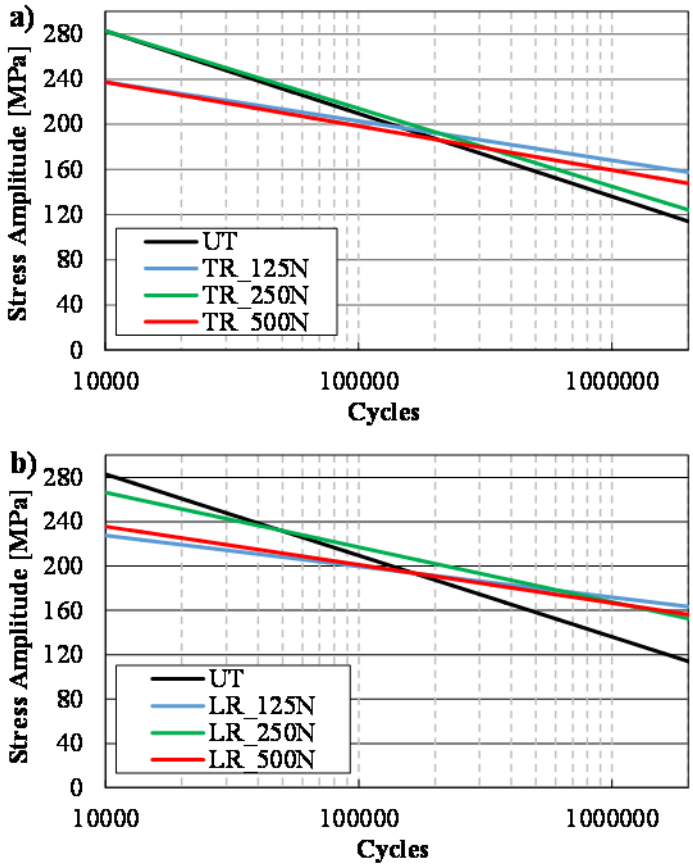

Figure 33 Wöhler Curves after Fatigue Test for 0.1 mm/pass Feed (a) TR (b) LR

Fatigue strength at 10^6 cycles is commonly used to quantify fatigue properties of materials. Table 4 shows the median fatigue strength values at 10^6 cycles for each case. It can be seen that up to 26% increase in fatigue strength could be achieved using deep rolling for 6082 aluminum alloy. Maximum increase in fatigue strength was obtained after 125 N LR with 172 MPa fatigue strength compared to 136 MPa for UT. In general, LR resulted in higher fatigue strength values compared to TR. This behavior can also be seen in Figure 34.

Table 4 Fatigue Strength Values at 10^6 Cycles for 0.1 mm/pass Specimens

	UT	**TR**			**LR**		
		125N	**250N**	**500N**	**125N**	**250N**	**500N**
Fatigue Strength [MPa]	136	168	145	159	172	167	167
Fatigue Strength Increase [%]	-	24	7	17	26	23	23

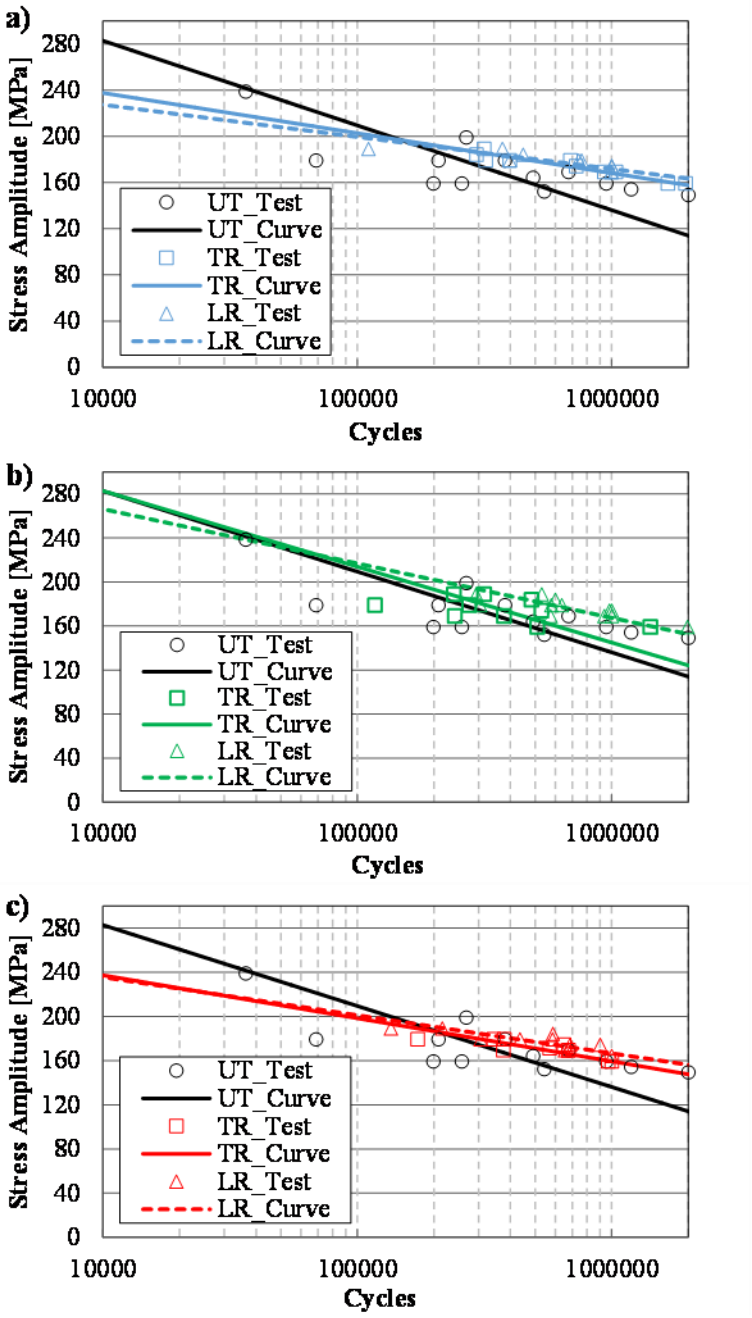

Figure 34 Comparison of Wöhler Curves for TR and LR (a) 125 N (b) 250 N (c) 500 N

Fatigue tests are prone to scatter and uncertainties. Therefore, statistical methods were used to quantify the effects of scatter. This procedure was explained under Section 4.1. Significant scatter can be observed in Figure 35 for UT specimen set. Therefore, lower bounds were considerably lower than median curve. Fatigue strengths of 87 MPa and 68 MPa were found at 10^6 cycles for R90C90 (90% reliability and 90% confidence interval) and lower 3-sigma, respectively. Median curve exhibited 136 MPa fatigue strength. This scatter can be attributed

to surface state of UT specimens, which were in as-turned state and significant irregularities were present at surface.

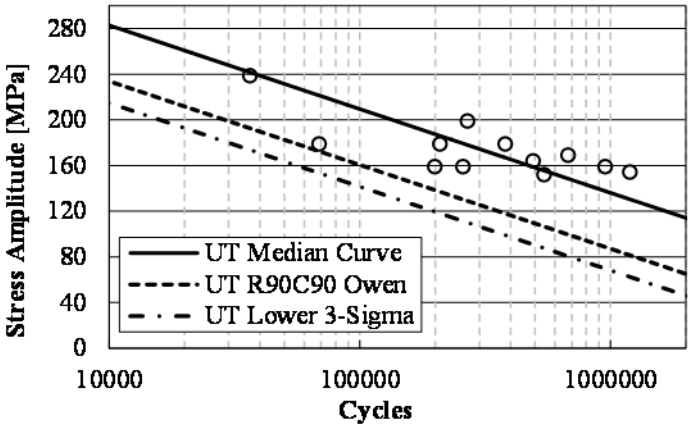

Figure 35 Lower Bounds for UT Set

Figures 36, 37 and 38 show lower bound curves together with median curves for 125 N, 250 N and 500 N DR sets with 0.1 mm/pass feed rate, respectively.

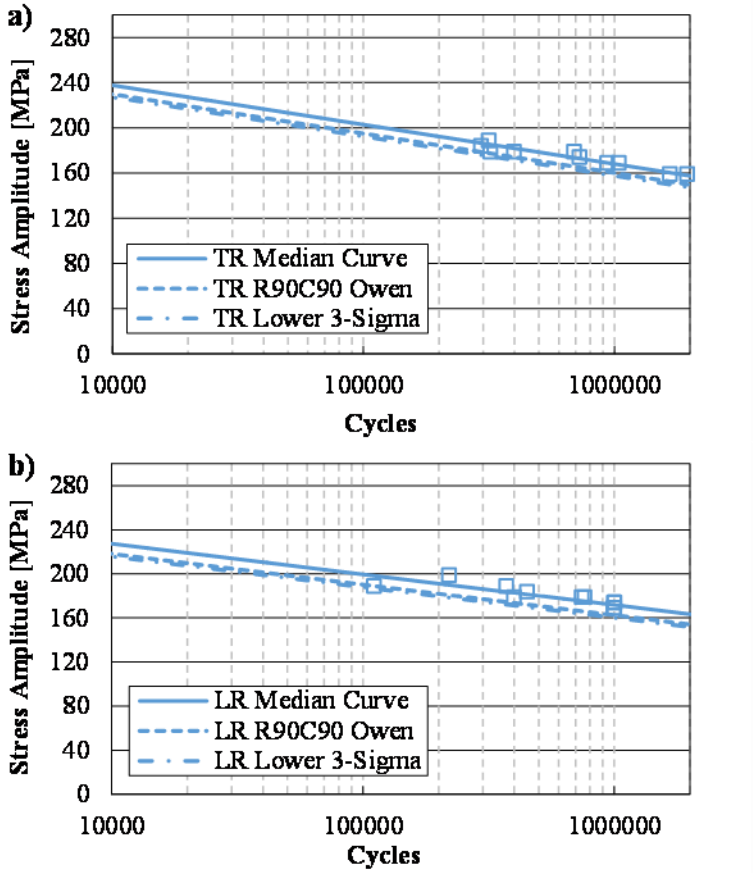

Figure 36 Lower Bounds for 125 N-0.1 mm/pass DR Set

From the figures, it can be seen that deep rolling resulted in less scatter compared to un-treated specimen set in general. Deep rolling results in reduced roughness and a regular surface, together with hardness increase and compressive residual stresses at surface. Therefore, probability of crack initiation decrease and both fatigue strength improvement and reduced uncertainties can be attained.

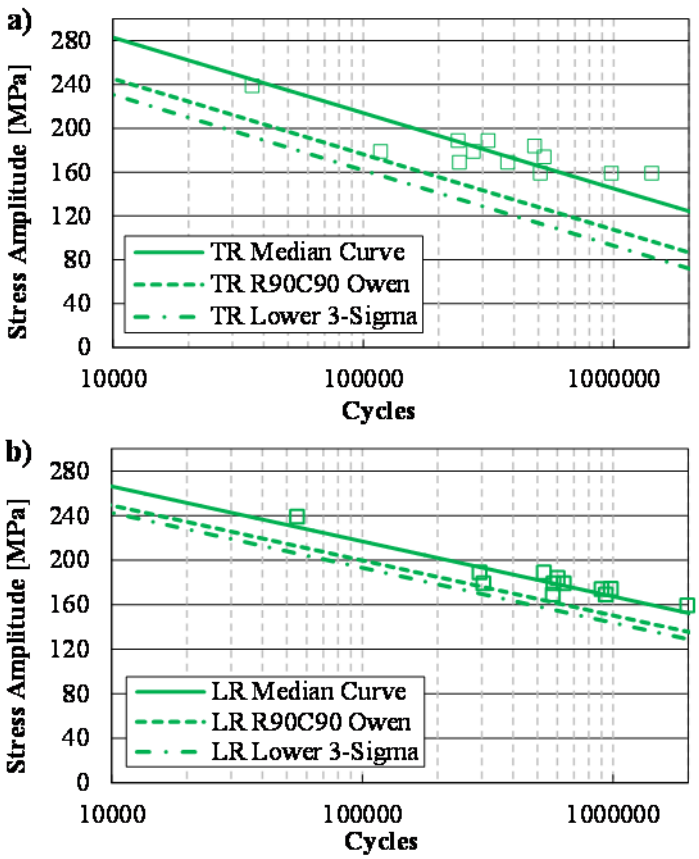

Figure 37 Lower Bounds for 250 N-0.1 mm/pass DR Set

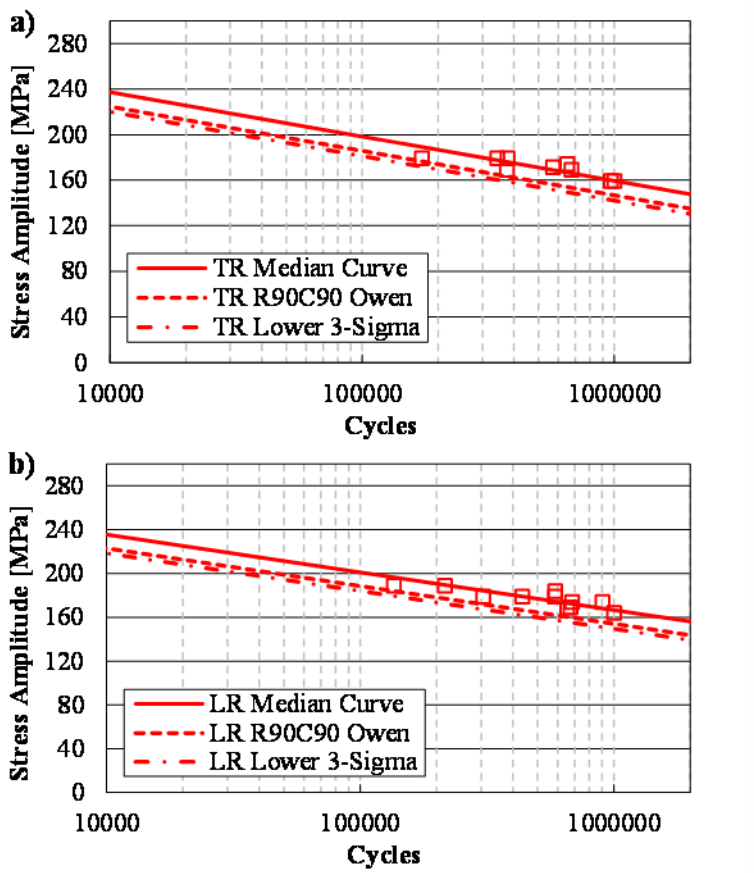

Figure 38 Lower Bounds for 500 N-0.1 mm/pass DR Set

Fatigue strength improvements became even more pronounced when lower bounds were considered. In component design, lower bounds are used since safety is a primary concern. Therefore, effect of DR on fatigue strength is crucial and significant improvement can be obtained in fatigue strength using it as seen in Table 5. Highest fatigue strengths for lower bounds were obtained using 125 N deep rolling. For example, for lower 3-sigma bound, 132% increase was calculated for 125 N LR compared to UT.

Table 5 Lower Bound Fatigue Strengths at 10^6 cycles for 0.1 mm/pass DR Specimens

	UT	TR			LR		
		125N	250N	500N	125N	250N	500N
Owen Fatigue Strength [MPa]	87	160	107	147	163	150	154
Owen Fatigue Strength Increase [%]	-	84	23	69	87	72	77
3-Sigma Fatigue Strength [MPa]	68	158	93	142	160	144	150
3-Sigma Fatigue Strength Increase[%]	-	132	37	109	135	112	121

Above results suggest that for each of the deep rolling forces, longitudinal rolling yielded better results compared to tangential rolling. This aspect of the current study shows that, for axisymmetric parts, changing the direction of deep rolling can affect the fatigue strengths positively. In industrial applications, increased fatigue life gives opportunity to use less material and reduce weight of already existing structures.

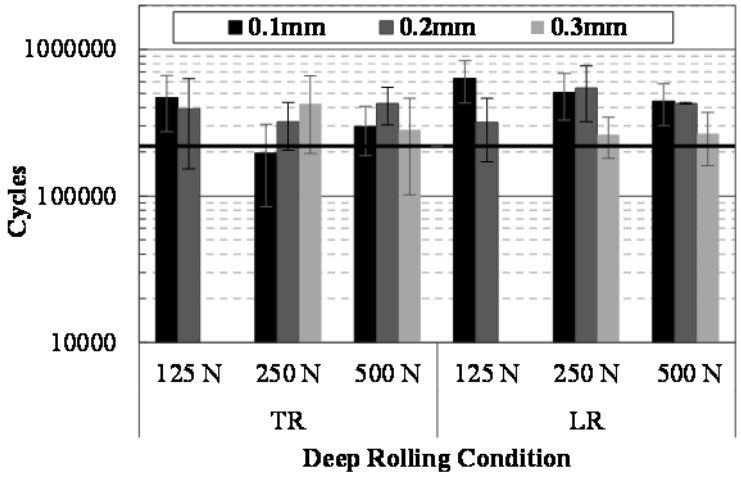

Figure 39 Fatigue Test Results at 180 MPa Stress Amplitude for Different Feed Rates

In industry, application speed is a crucial parameter for feasibility of the process within the production chain. Feed rate is the main limiting factor for speed of deep rolling operation. Because of this, fatigue tests were conducted with different feed rates using stress amplitude of 180 MPa for at least 3 specimens for each case. Results can be seen in Figure 39. Horizontal black line represents mean UT specimen life of 219025 cycles. Feed rate increase for DR with 125 N force resulted in reduction in life and significant increase in scatter. Therefore, higher feeds tan 0.1 mm/pass were found to be not feasible for 125 N DR. However, for higher forces, higher feed rates can be used to improve fatigue life. Reason for this is the higher plastic deformations and bigger deformation area under high forces compared to low force applications. For example, 500 N TR with 0.2 mm/pass feed resulted in 428009 cycles life with acceptable scatter. For LR, both 250 N and 500 N rolling with 0.2 mm/pass feed can be used to increase fatigue life. Especially 500 N LR with 0.2 mm/pass exhibited almost no scatter and was a favorable option to apply deep rolling. However, care should be taken to analyze the results in Figure 39, as Wöhler curves were not completely derived. More tests should be done at different stress amplitudes and Wöhler curves should be obtained to get useful and safe data.

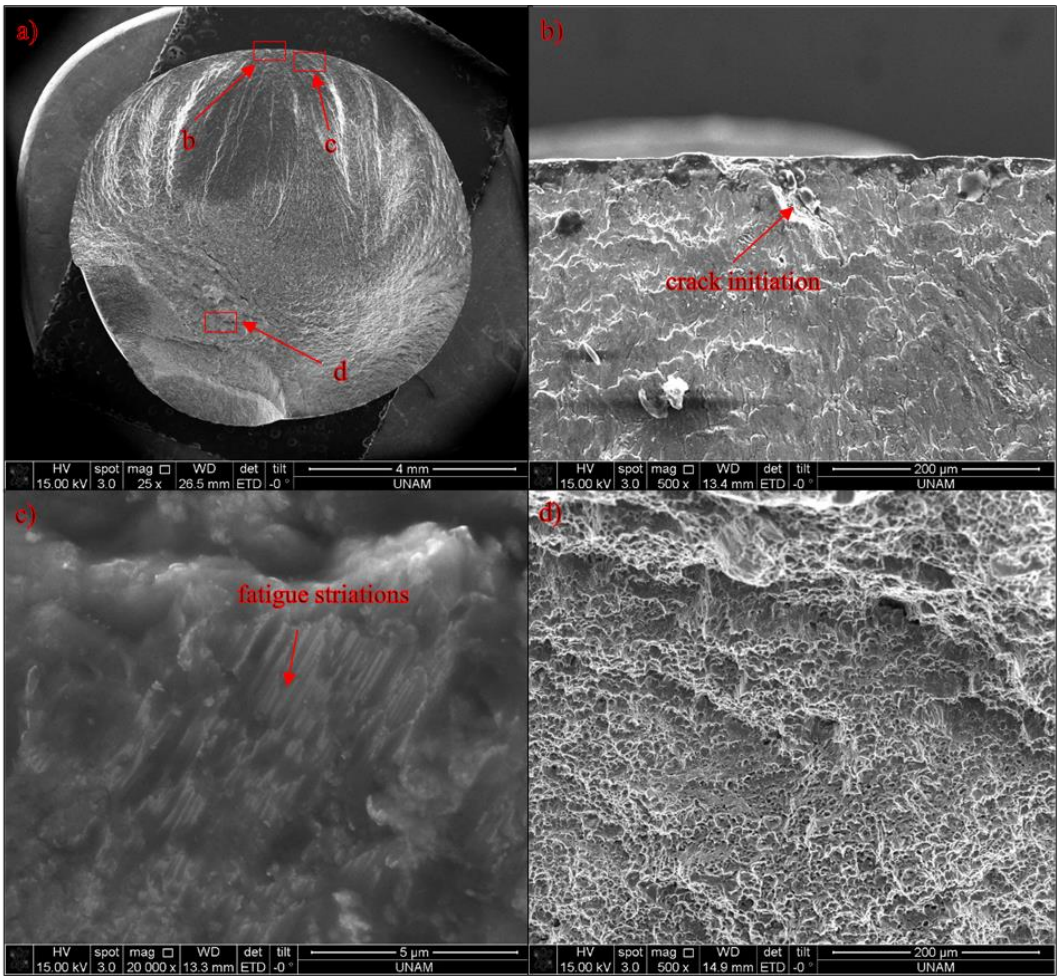

Figure 40 SEM Images of UT Specimen Fractured under σ_a = 160 MPa (a) General view (b) Crack Initiation Zone (c) Fatigue Striations Close to Crack Initiation Zone (d) Sudden Fracture Zone

SEM images of UT, TR and LR specimens were presented in Figures 40, 41 and 42. TR and LR specimens had DR force of 250 N and feed of 0.1 mm/pass. Crack initiation at surface can be seen in Figure 40(b) for UT specimen. This was expected, since fatigue cracks usually starts at free surface where irregularities and defects are present. After initiation, propagation of crack took place. This can be seen in Fig 40(c). After reaching a critical length, remaining material could not resist the load and specimen failed catastrophically. Sudden fracture zone can be seen in Fig 40(d).

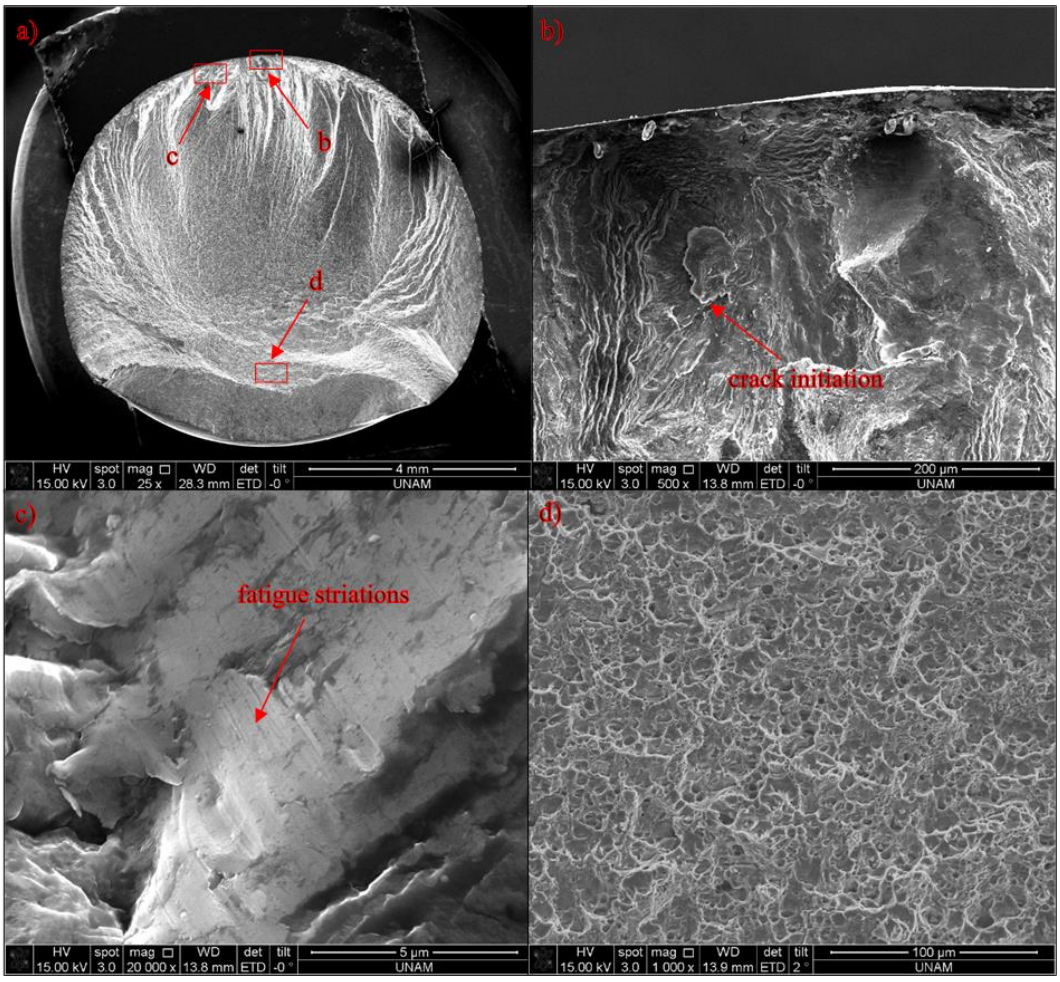

Figure 41 SEM Images of TR-250N-0.1mm/pass Specimen Fractured under σ_a = 160 MPa (a) General view (b) Crack Initiation Zone (c) Fatigue Striations Close to Crack Initiation Zone (d) Sudden Fracture Zone

Contrary to UT specimen, both TR and LR specimens exhibited somewhat sub-surface crack initiation as shown in Figure 41(b) and 42(b). TR specimen crack initiation was found to be at approximately 0.2 mm depth compared to 0.4 mm for LR one. Around the crack initiation sites, there was a wave-like texture. This kind of texture was not observed in UT specimen. This texture is believed to be result of shear deformation pile-ups and persistent slip band deepening. The fact that these textures formed and crack initiated at sub-surface region indicates that crack initiation was delayed for a considerable amount of time. Since Stage-I crack growth behavior usually takes most of the time of fatigue life for high-cycle fatigue [24], fatigue life improvement was mainly attributed to this phenomenon.

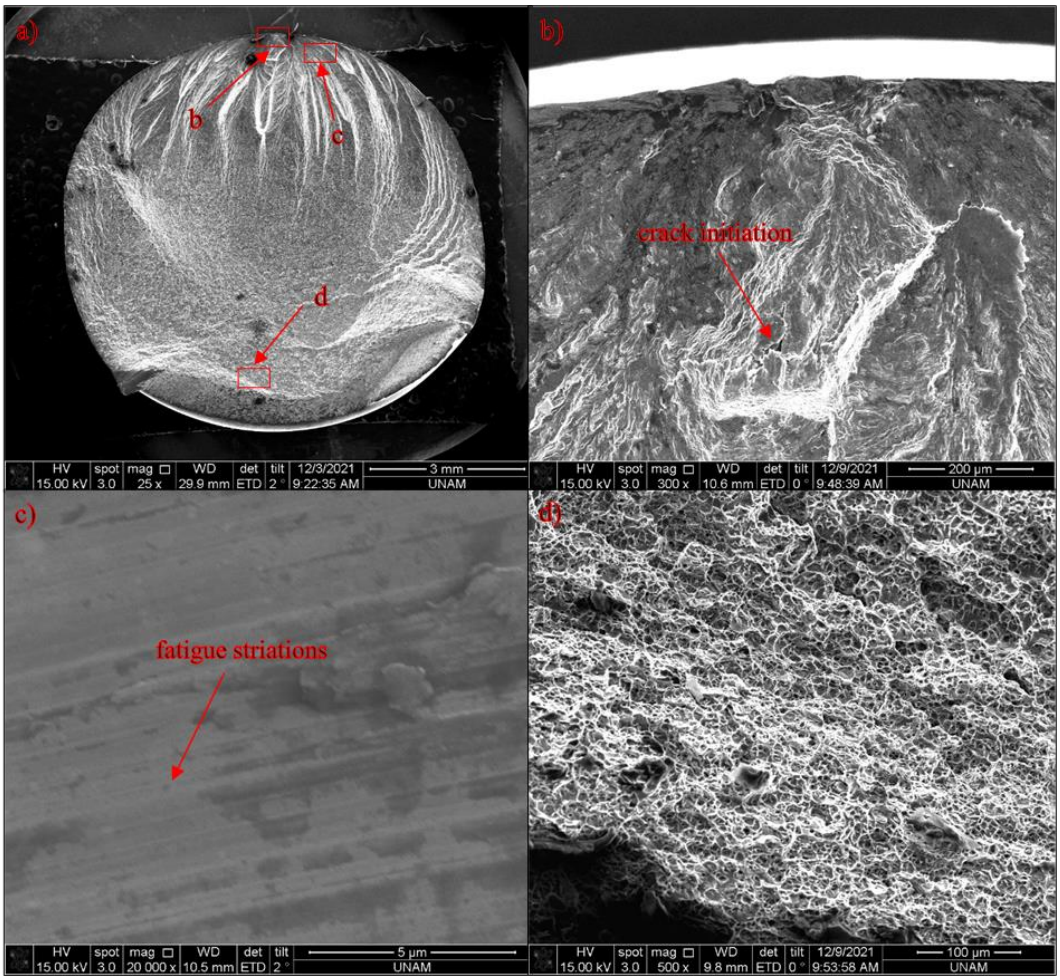

Figure 42 SEM Images of LR-250N-0.1mm/pass Specimen Fractured under σ_a = 160 MPa; (a) General view (b) Crack Initiation Zone (c) Fatigue Striations Close to Crack Initiation Zone (d) Sudden Fracture Zone

6. CONCLUSIONS AND OUTLOOK

In this study, fatigue improvement by means of deep rolling of EN-AW 6082 aluminum alloy was investigated for asymmetrical specimens. Firstly, T6 heat-treatment of 6082 aluminum alloy was studied. Solution heat treatment temperature was found to be critical for strength after artificial aging and higher SHT temperatures resulted in higher strengths. Therefore 550°C for 90 minutes was selected for SHT procedure. During artificial aging, strength increases were faster for higher AA temperatures and times as low as 1 hour can be employed to obtain 300 MPa yield strength at temperatures higher than 200°C. Highest strength values were achieved using 240min-200°C AA. Notwithstanding, 480min-180°C AA was used throughout the study as this AA schedule resulted in optimal strength and ductility properties.

Deep rolling was employed using spring loaded, roller type deep rolling tool. 125 N, 250 N and 500 N rolling forces were used for different feed rates. For roughness, hardness and fatigue measurements, 8 mm diameter specimens were used. However, residual stress measurements were done on flat specimens since hole drilling method can only be accurately used on flat surfaces to measure residual stresses. It was found that deep rolling resulted in significant roughness decrease, which is beneficial for fatigue life. Dependency of roughness on feed rate was found to be significantly higher than rolling force. For tangential rolling, roughness was mainly controlled by feed rate. However, for longitudinal rolling; effect of rolling force was more pronounced since LR procedure was discrete in nature. Hardness measurements indicated that near-surface region of deep rolled specimens were plastically deformed sufficiently and work-hardened for 250 N and 500 N forces with 0.1 mm/pass feed. Approximately 10% hardness was reported at surface. Residual stress measurements were done on flat surface and up to 0.4 mm depth for 0.1 mm/pass feed specimens for every force. It was shown that, all DR applications resulted in compressive residual stresses in the vicinity of surface. Minimum residual stress (maximum compressive) was formed after some depth for each case. As deep rolling forces increased, residual stresses became more negative (more compressive) and depth of minimum residual stresses were increased. These compressive residual stresses are known to be beneficial for fatigue strength.

Fatigue tests were conducted on UT, TR and LR specimens for 0.1 mm/pass feed rate for each force at first. After Wöhler curves of these specimen sets were formed, investigations were done using higher feed rates. It was shown that both TR and LR increased fatigue strength compared to UT. For each force, LR resulted in higher fatigue strengths at 10^6 cycles than TR. These results confirm the measurements of compressive residual stresses shown in Figure 32. In LR, rolling direction is the direction of longitudinal axis of specimen. This direction was fatigue-loading direction. Therefore higher compressive residual stresses in rolling direction as shown in Figure 32(a) are expected to increase fatigue strength by diminishing the effects of tensile loadings. Up to 26% increase in fatigue strength could be achieved using 125 N 0.1 mm/pass LR. Therefore, it can be said that, LR is a beneficial and promising method to employ on axisymmetric industrial components. Statistical lower bound curves indicated that fatigue strength improvements were even more obvious after DR compared to UT specimen set when lower bounds were used. This is because of much lower scatters of fatigue data after DR compared to UT specimen set. For high force DR applications, higher feed rates may be used to improve fatigue strength. This would be beneficial since it would reduce time needed to manufacture components. This was especially true for LR where both 250 N and 500 N LR at 0.2 mm/pass improved fatigue properties considerably.

Scanning electron microscopy images showed that fatigue cracks form at surface for UT specimens. In contrast, crack initiation was shifted toward sub-surface regions for both TR and LR. This phenomenon was shown for 250 N 0.1 mm/pass DR specimens. Since fatigue crack initiation was shifted toward interior, it can be said that crack initiation phase was delayed.

Above results show that, LR can be used to improve fatigue properties of industrial components instead of TR. In future works, Wöhler curves of higher feed rate DR applications are to be determined. In addition, LR application of different materials can be studied and validation of LR as a new approach of DR can be made.

REFERENCES

[1] World Steel Association. "Advanced High-Strength Steel Applications Guidelines Version 6.0". http://www.worldautosteel.org/projects/advanced-high-strength-steel-application-guidelines (Son Erişim Tarihi:14.08.2017)

[2] Kleiner. M., Geiger, M., Klaus, A, CIRP Annals – Manufacturing Technology, 52-3 (**2003**) 521-542.

[3] L. Kukielka, Journal of Mechanical Technology, 19 (**1989**) 319-356.

[4] G. Lütjering and J. Williams, Titanium, Berlin-Heidelberg-New York: Springer, **2007**

[5] K. Kirkhope, R. Bell, L. Caron, R. Basu and K.-T. Ma, Marine Structures, 12 (**1999**) 447-474.

[6] Wagner. L, Materials Science and Engineering A, 263 (**1999**) 210-216.

[7] V. Schulze, Modern Mechanical Surface Treatment, Weinheim: WILEY-VCH, **2006**.

[8] B. Scholtes and O. Voehringer, Mechanical Surface Treatment, Amsterdam: Elsevier, **2001**, 5253-5261.

[9] H. Maio, D. Demers, S. Larose, C. Perron and M. Levesque, Journal of Materials Processing Technology, 210 (**2010**) 2089-2102.

[10] S. Bagherifard, I. Fernandez-Pariente, R. Ghelichi and M. Guagliano, International Journal of Fatigue, 65 (**2014**) 64-70.

[11] A. H. Clauer, "Laser Shock Peening for Fatigue Resistance," *LSP Technologies, Inc.*, **1996.**

[12] Chahardehi, A., Brennan, F.P., Steuwer, A, Engineering Fracture Mechanics, 77 (**2010**) 2033-2039.

[13] Gujba, A.K., Medraj, M, Materials, 7(12) (**2014**) 7925-7974.

[14] Wagner, L., Mhaede, M., Wollmann, M., Altenberger, I., Sano, Y, International Journal of Structural Integrity 2(2) (**2011**) 185-199.

[15] Richards, M.D., Burnett, M.E., Speer, J.G., Matlock, D, Metallurgical and Materials Transactions A, 44 (**2013**) 270-285.

[16] Prabhu, P.R., Kulkarni, S.M., Sharma, S, Journal of Materials Research and Technology, 9(5) (**2020**) 11402-11423.

[17] Lambda Technologies Group. "Laser Shock Peening". https://www.lambdatechs.com/laser-peening/ (Son Erişim Tarihi 21/04/2022).

[18] Y. Birol, E. Gokcil, M. A. Guvenc, S. Akdi, Materials Science and Engineering A, 674 (**2016**) 25-32.

[19] A. Cuniberti, A. Tolley, M.V. Castro Riglos, R. Giovachini, Materials Science and Engineering A, 527 (**2010**) 5307-5311.

[20] F. Ozturk, A. Sisman, S. Toros, S. Kilic, R.C. Picu, Materials and Design 31 (**2010**) 972-975.

[21] G. Mrówka-Nowotnik, J. Sieniawski, A. Nowotnik, Journal of Achievements in Materials and Manufacturing Engineering, 17 (**2006**) 105-108.

[22] G. A. Edwards, K. Stiller, G. L. Dunlop, M. J. Couper, Acta Materialia 46 (**1998**) 3893-3904.

[23] M. W. Zandbergen, Q. Xu, A. Cerezo, G. D. W. Smith, Acta Materialia 101 (**2016**) 136-148.

[24] Dieter, G.E., Bacon, D, Mechanical Metallurgy (Metric Edition), McGraw-Hill: United Kingdom, **1988**.

[25] Wöhler, A, Zeitschrift für Bauwesen, 20 (**1870**) 73–106.

[26] ASTM 606-04 Standard Specification for Steel, Sheet and Strip, High-Strength, Low-Alloy, Hot-Rolled and Cold-Rolled, with Improved Atmospheric Corrosion Resistance

[27] T. Ludian and L. Wagner, V. Schulze (Chairman), International Scientific Comittee on Shot Peening: Shot Peening, Paris, **2005**.

[28] M. D. Sangid, International Journal of Fatigue, 57 (**2013**) 58-72.

[29] M. Su, L. Xu, C. Peng, Y. Han, L. Zhao, International Journal of Fatigue 156 (**2022**) 106689.

[30] Y. F. Al-Obaid, Mechanics of Materials, 19 (**1994**) 251-260.

[31] N.R. Tao, M. Suib., J. Lud and K. Lua, Nanostructured Materials, 11(4) (**1999**) 433-440.

[32] Dane, C.B., Hackel, L.A., Haly, J., Harrison, J, Advanced Materials and Processes 153 (**1998**) 37-38.

[33] R. K. Nalla, I. Altenberger, U. Noster, G. Y.Liu, G. Y. Scholtes, R. O. Ritchie, Material Science and Engineering A, 355 (**2003**) 216-230.

[34] P. Delgado, I. Cuesta, J. Alegre and A. Díaz, Presicion Engineering, 46 (**2016**) 1-10.

[35] C. C. Wong, A. Hartawan, W. K. Teo, Proceedia CIRP, 13 (**2014**) 350-354.

[36] A.M. Abrao, B. Denkena, J. Köhler, B. Breidenstein,T. Mörke, P.C.M. Rodrigues, Journal of Materials Processing Technology, 214 (**2014**) 3020-3030.

[37] M. Abdulstaar, M. Mhaede and L. Wagner, Advanced Engineering Materials, 15 (**2013**) 1002-1006.

[38] M. Beghini, L. Bertini, B. Monelli, C. Santus and M. Bandini, Surface & Coatings Technology, 254 (**2014**) 175-186.

[39] M. Sticchi, D. Schnubel, N. Kashaev, N. Huber, Applied Mechanics Review, 67(1) (**2015**) 1-9.

[40] I. Altenberger, R. K. Nalla, Y. Sano, L. Wagner, R. O. Ritchie, International Journal of Fatigue, 44 (**2012**) 292-302.

[41] P. Prevey and J. Cammett, International Journal of Fatigue, 26 (**2004**) 975-982.

[42] V. Backer, F. Klocke, H. Wegner, A. Timmer, R. Grzhibovskis and S. Rjasanow, IOP Conference Series: Materials Science and Engineering, 10 (**2010**) 1-10.

[43] H. Coules, G. Horne, S. Kabra, P. Colegrove and D. Smith, Journal of Manufacturing Processes, 26 (**2017**) 240-251.

[44] Y. Lee, J. Pan, R. Hathaway, M. Barkey, Fatigue Testing and Analysis: Theory and Practice. 1st edn. Elsevier Butterworth-Heinemann, Burlington, **2004**.

[45] C. R. Williams, Y. Lee, J. T. Rilly, International Journal of Fatigue, 25 (**2003**) 427-436.

[46] I. Dutta, S. M. Allen, Journal of Materials Science Letters, 10 (**1991**) 323-236.

[47] G. Majzoobi, K. Azadikhah and J. Nemati, Materials Science and Engineering A, 516 (**2009**) 235-247.